WATER BALANCE CONSIDERATIONS IN MODELING OF PEM FUEL CELL SYSTEMS

By

ROHIT M. SHARMA

A THESIS PRESENTED TO THE GRADUATE SCHOOL
OF THE UNIVERSITY OF FLORIDA IN PARTIAL FULFILLMENT
OF THE REQUIREMENTS FOR THE DEGREE OF
MASTER OF SCIENCE

UNIVERSITY OF FLORIDA

2005

This document is dedicated to my parents who have supported me in all my endeavors

ACKNOWLEDGMENTS

First of all, I would like to thank Dr. William. E. Lear, the chairman of my graduate committee, for providing me with an opportunity to work under his guidance as a part of the fuel cell lab. Dr. Lear shared with me his extensive knowledge and always motivated me to perform better. I would also like to thank Dr. James Fletcher, the co-chair of my committee, for his efforts. It was fun working under his guidance as he shared a lot of his experiences. I would also like to acknowledge Dr. Herbert Ingley for being a part of my committee and for the time and support that he provided.

In addition, I would like to thank the members of the fuel cell lab and my friends and colleagues for their support.

Above all I would like to express my gratitude to my parents for their unwavering support and blessings.

TABLE OF CONTENTS

LIST OF TABLES

LIST OF FIGURES

KEY TO SYMBOLS
NOMENCLATURE

$\dot{m}$	mass flow rate of water
N	molar flow rate
y	fraction of excess air
M	molecular weight
M'	non-dimensional mass flow rate
p	pressure
R	gas constant
T	temperature
a	constant in Redlich-Kwong equation
b	constant in Redlich-Kwong equation
g	gibbs free energy
f	fugacity
N	rotational speed of a compressor
F	faraday's constant
ń	number of cells in a fuel cell stack
n	number of electrons transferred in an electrochemical reaction
I	fuel cell stack current
v	velocity

$\dot{m}$	mass flow rate of air
V	Volume
A	Area

Greek

Φ	relative humidity of ambient air
υ	specific volume
η	efficiency of water separator
Θ	ratio of inlet air temperature to reference temperature in a compressor
δ	ratio of inlet air pressure to reference pressure in a compressor
γ_1	ratio of dimensional parameters of a compressor
χ	mole fraction
ρ	density

Subscripts

H_2O-in	water that enters the control volume
H_2O-out	water that leaves the control volume
H_2O-gen	water generated inside the control volume
H_2O-excess	excess water leaving the control volume
mem	water supplied back to the stack
liquid-out	liquid water leaving the control volume along with exit air
design	design point
excess	excess water leaving the control volume
amb	ambient
r	ratio

t	exit air properties
1	saturated exit air properties
2	modified saturated exit air properties
real	real gas properties
liq	liquid
c	critical
correct	corrected properties of gas
a	actual properties of gas
humid	properties of humidified air
H_2O -90%	properties of vapor present in 90% humidified air
dry	dry conditions (relative humidity is zero)

Abstract of Thesis Presented to the Graduate School
of the University of Florida in Partial Fulfillment of the
Requirements for the Degree of Master of Science

WATER BALANCE CONSIDERATIONS IN MODELING OF PEM FUEL CELL SYSTEMS

By

Rohit M. Sharma

August 2005

Chair: W. E. Lear
Co-chair: J. Fletcher
Major Department: Mechanical and Aerospace Engineering.

In order for the potential of proton exchange membrane (PEM) fuel cells to be realized for automotive applications, several important system-level issues must be solved. One of the requirements placed on automobile engine operation is to operate satisfactorily under a wide range of ambient conditions and power demands. Under some combinations of temperature, altitude, and load, the mass rate at which liquid water is recovered by the fuel cell system is less than the mass rate of water required to humidify the membranes. Unless significant liquid water reserves are carried – not an attractive design option – then the membranes will become dry, with potential catastrophic results. In this study, an analysis is shown which allows the water discharge rate to be calculated as a function of ambient conditions and operating parameters such as overall stoichiometry, operating pressure and exhaust temperature. The analysis is design-independent, in that specific design choices only affect the inputs to the model such as air fuel stoichiometry and exhaust temperature and pressure parameters. The condition of

zero net water discharge is emphasized, since that corresponds to the boundary between sufficient water and the catastrophic dry-out process. Results indicate that moderate-to-high altitude operation will most likely require pressurization of the fuel cell stack.

The operating parameters of non-ideal components and subsystems change under varying operating conditions, which imposes additional limitations on achieving water balance. The effect of these limitations associated with the air delivery sub-system and water recovery components has been studied by considering certain specific design and equipment choices and analyzing their effect on water balance under varied ambient and operating conditions. The results of this portion of study indicate that the efficiency of the water recovery subsystem, in addition to ambient and operating parameters, affects the water balance of the fuel cell system. The magnitude of this effect is however design dependent and should be taken into account when considering a specific arrangement. The effect of using a non-ideal air handling subsystem such as a centrifugal compressor is that the water discharge rate reduces when the fuel cell operates at part load conditions; however the effect is more profound for lower fractions of design load.

CHAPTER 1
INTRODUCTION

With a growing emphasis on the preservation of our environment, air pollution has become a focus of concern. Significant contributors to air pollution are the conventional vehicles that operate on petroleum. In the United States, they are responsible for over 60 percent of the carbon monoxide emissions and about 20 percent of greenhouse gas emissions.

A conscious effort has been made over the past few decades to develop an alternate fuel for transport applications. Use of hydrogen to operate a fuel cell promises to be a clean and efficient solution to the problem. Fuel cell based vehicles have the potential of producing lower emission than their petroleum based counterparts. However fuel cell technology is still in its development stages and there are certain design issues that need to addressed in order to ensure reliable and efficient operation under varied operating conditions.

1.1 Fuel Cells Basics

Fuel cells produce electricity by utilizing the chemical energy released when hydrogen combines with oxygen to form water. The overall reaction is as follows:

$$H_2 + \frac{1}{2} O_2 \rightarrow H_2O \qquad 1\text{-}1$$

Hydrogen is supplied to the anode where it splits into H^+ ions and electrons in the presence of a catalyst. The electrons travel via the external circuit towards the cathode. The charge that is transferred across the external circuit, for each mole of diatomic

hydrogen oxidized, is the product of the number of electrons transferred in the electrochemical reaction, and the Faraday constant. The H^+ ions migrate to the cathode via the electrolyte where they combine with the oxidant and the electrons to form water.

Based on the Nernst equation,[1] the potential generated by a fuel cell operating on hydrogen is given by the following equation:

$$E = E^\circ - \left(\frac{RT}{nF}\right)\ln\left(\frac{p_{H_2} \cdot p_{O_2}^{1/2}}{p_{H_2O}}\right) \qquad 1\text{-}2$$

where E° is the EMF of the cell under standard conditions and its value is 1.229 V when the product of the reaction is liquid water and 1.18 V when the product is gaseous water.[2] The remaining part of equation 1-2 takes into account the change in the cell voltage from its standard value due to changes in temperature of the reaction or change in partial pressures of the reactants or the products. R is the universal gas constant, T is the temperature of the reaction, n is the number of electrons transferred for each mole of fuel utilized, F is the Faraday constant and p_{H_2}, p_{O_2} and p_{H_2O} are the partial pressures of hydrogen, oxygen and water respectively.

Based on this expression and Equation 1-2, one would expect the value of voltage developed by the fuel cell for different values of current to be constant at constant operating pressure and temperature. However, the actual value of cell potential decreases due to certain irreversible losses. These losses originate primarily from three sources: (1) activation polarization (2) ohmic polarization, and (3) concentration polarization.[3] Activation polarization is predominant at low current densities and is related to the rate of the electrochemical reaction. Ohmic polarization losses take place due to the resistance offered by the electrolyte to the flow of ions and the resistance to the flow of electrons

through the electrode material. Its value increases with the increase in current, mainly because the resistance of the cell remains more or less constant over the entire range of current. Concentration polarization is caused due to a concentration gradient that develops near the electrode when the reactant material is consumed and the surroundings are unable to maintain the initial concentration. It mainly results from the slow transport of reactants/products to/from the electrochemical reaction site and has a more pronounced effect at higher values of current.

The above-mentioned losses affect the voltage versus current characteristics, defined as "polarization curve," of a fuel cell. Figure 1-1 shows a typical polarization curve of a fuel cell.

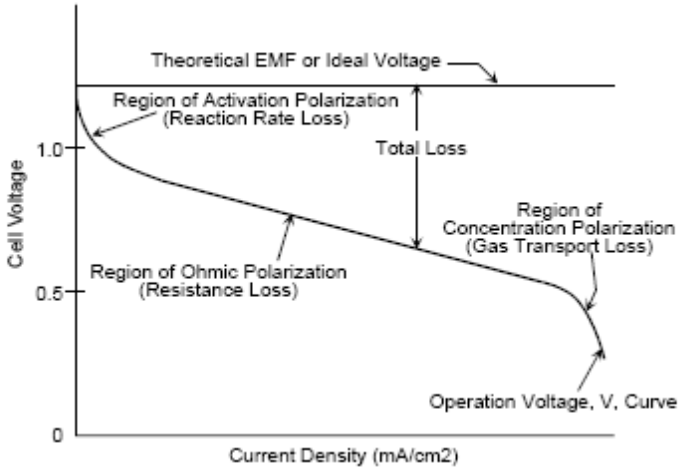

Figure1-1. Cell voltage v/s current density for a general fuel cell.[3] (Source: EG & G Services Parson Inc., Fuel Cell Handbook, 5th edition, U.S. Department of Energy, National Energy Technology Laboratory, 2000)

1.2 Type of Fuel Cells

Different types of fuel cells are available as a potential source of clean and efficient energy. Amongst the more common ones are alkaline fuel cell (AFC), phosphoric acid fuel cells (PAFC), molten carbonate fuel cell (MCFC), solid oxide fuel cells (SOFC) and proton exchange membrane cells (PEMFC). This section discusses in brief the above-

mentioned fuel cell types with a greater emphasis on PEM based fuel cells. It also gives the rationale behind the popularity of PEM based fuel cell in automotive applications.

1.2.1 Phosphoric Acid Fuel Cells (PAFC)

Phosphoric acid fuel cells, as the name suggests, use phosphoric acid (H_3PO_4) as an electrolyte. These fuel cells operate at a temperature of around 200°C.

PAFCs, in general, are not very suitable for low to medium power automobiles because of their low power to weight ratio and high operating temperatures which result in longer system startup times. Moreover, the presence of a liquid electrolyte in the fuel cell increases the chances of acid spillage and poses a limitation on the orientation of the cell. However the electrolyte does not need humidification to maintain its conductivity. These cells are generally used in stationary power applications and sometimes in large vehicles such as buses where size and weight are not major limitations.

1.2.2 Alkaline Fuel Cells (AFC)

These fuel cells use an alkaline solution as an electrolyte, generally potassium hydroxide (KOH) or sodium hydroxide (NaOH) with a concentration of 85 wt%. The normal operating temperature of these fuel cells is around 250°C.

The main drawback of AFCs is that hydrogen and oxygen have to be supplied to the cell in pure form. Another option is to supply "scrubbed fuel and oxidizer (air)" to the anode and cathode respectively.[5] This requirement makes the auxiliaries of the fuel cell more complex and high in weight and volume. A high operating temperature means slower system startup, costlier material of construction and complex manifolds and bends that are added to the system due to the requirement of an active cooling system. Moreover, as in case of PAFC, the liquid form of the electrolyte poses a limitation on the

orientation of the cell. The liquid electrolyte on the positive side does not need humidification for efficient operation.

1.2.3 Molten Carbonate Fuel Cells (MCFC)

These cells use a mixture of molten alkali carbonates as an electrolyte. The electrolyte is retained in a ceramic matrix of lithium aluminum oxide ($LiAlO_2$). These fuel cells normally operate at a high temperature of around 600 to 700 °C.

From a commercial applications point of view, MCFCs have an efficiency approaching 60% which is considerably higher than the efficiency of PAFCs. The conductivity of the membranes of MCFCs is not dependent on the humidity of the membranes. Moreover, these cells can directly use a high density hydrocarbon fuel. However, very high operating temperatures make them unfavorable for use in automotive applications like cars. These cells are more suited for stationary applications. When the waste heat of these cells is utilized by a power plant to generated additional electricity, the overall efficiency of the system reaches close to 85%.

1.2.4 Solid Oxide Fuel Cells (SOFC)

Solid oxide fuel cells use a non-porous ceramic compound, generally yttria-stabilized zirconia (YSZ) as an electrolyte. These cells normally operate at a very high temperature of about 1000 °C.

A high operating temperature gives these fuel cells the capability to internally reform a hydrocarbon fuel to hydrogen. SOFCs like the fuel cell types discussed above do not require water to maintain the conductivity of the membranes. Hence, overall water balance of the fuel cell system does not affect its performance. Moreover, these fuel cells are more resistant to impurities than any other fuel cell. The disadvantages of operating close to 1000 °C are high thermal stresses that impose limitations on the construction

material and the design of its auxiliaries, slow system startup, heavier and costly insulation and higher chances of material corrosion.

1.2.5 Proton Exchange Membrane Fuel Cells (PEMFC)

These fuel cells use a solid proton conducting membrane, generally made of sulphonated fluro-polymers, as an electrolyte. One such commercially available product is Nafion® (DuPont). The electrolyte is sandwiched between two electrodes that are made of platinum impregnated porous carbon. Platinum dispersed in the electrodes acts as a catalyst and aids the electrochemical reaction. The back of the electrodes are generally coated with a hydrophobic compound such as PTFE. The hydrophobic coating on the porous electrodes removes water from the catalyst sites and aids the reactant gases to diffuse onto the catalyst.

The normal operating temperature of PEM fuel cells is around 80°C. Increasing the fuel cell temperature shifts the polarization curve to higher values of voltage and thus increases the cell performance. However, high operating temperatures dehydrates the electrolyte and reduces its conductivity. Therefore PEM fuel cells are operated at a temperature 20°C less than the boiling point of water corresponding to the cell operating pressure. Increasing the fuel cell pressure increases its reversible potential. However, high operating pressures require higher compressor power.

The use of a solid electrolyte reduces the ohmic loses in the fuel cell and makes the cell more compact. As a result PEM fuel cells have a high power to weight and power to volume ratio. Moreover a solid electrolyte does not place a limitation on the orientation of the fuel cell as there is no problem of electrolyte spillage. The operating temperature of these fuel cells is much lower than the normal temperature of other fuel cell types. As a result the heat removal system is much lighter and less complex in PEM fuel cell systems

than in other fuel cell types. It also reduces component wear and increases the available range of materials for construction. This again decreases the size and cost of the system. A lower operating temperature in comparison to other fuel cells results in comparatively fast system startup time. Moreover these cells are able to sustain operation at high current densities. All these advantages make PEM fuel cells more favorable for automotive applications than other fuel cells.

Despite its advantages, PEM fuel cells have certain drawbacks that impose limitations on the design of the overall system. Platinum, which is used as a catalyst, is sensitive to CO poisoning. Carbon monoxide strongly bonds to platinum at temperatures less than 150°C and makes them unavailable as catalysts. Hydrogen reformed from hydrocarbons generally contains greater than one percent carbon monoxide, whereas, a concentration of greater than 10 ppm of CO is able to poison the catalyst.[5] Hence an additional reactor to reduce the amount of CO in the fuel gas is required if hydrogen is produced by an on-board fuel reformer.

Another drawback specific to automotive applications is fuel storage. Hydrogen if stored on-board an automobile as pure compressed gas, must be carried along in large volumes in order to achieve a reasonable travel distance. This is because of the low density of hydrogen. Use of high density hydrocarbons, such as methanol, as fuel decreases the storage volume but increases the cost and maintenance requirements of installing an additional reformer. Moreover, adding a reformer increases the overall weight of the fuel cell system. Hence a proper design choice must be made when deciding on the mode of fuel supply.

Last but not the least, and probably the one of the more important drawbacks related to PEM fuel cells, is maintaining water balance. This issue will be discussed in depth in the following section.

1.3 Water Balance in PEM Fuel Cells

The conductivity of the proton exchange membrane is directly proportional to the amount of water present in it. Absence of water in the membranes causes what is known as ‘membrane dry out’, where the electrolyte stops conducting protons. On the other extreme, too much water in the membranes causes flooding, where the pores in the electrodes are blocked by water. Flooding of the electrode pores prevents the reactant gases from coming in contact with the catalyst and hence inhibits the rate of the electrochemical reaction.

The total water present in the fuel cell does not indicate the local condition of the membranes. Even though sufficient water may be present in the fuel cell to humidify the membranes, some parts of the membrane may be flooded while others may be deficient or even dry. There are multiple reasons for this effect, of which the most common one is the inability of the water generated at the cathode to diffuse towards the anode. This makes the portion of the membranes near the cathode wet and the one near the anode dry. Another reason is due to “electro-osmotic drag” where the H^+ ions moving from the anode towards the cathode pull water molecules along with them, making the anode dry. In general, a drop in the quantity of water in the fuel cell stack indicates loss of water content of the membranes. This condition should be avoided in all cases to prevent membrane dry-out.

Water enters the fuel cell in the form of vapor as a part of the moist air supplied to the cathode and sometimes along with the hydrogen, which may be humidified depending

upon the overall system design. Water is constantly generated, due to the electrochemical reaction, at a rate which depends upon the amount of fuel used. The air leaving the fuel cell entrains liquid water along with it and at times, depending upon the operating temperature and pressure, evaporates water present in the membranes. Water is also lost due to leakage in different components present in the overall system. The net water present in the fuel cell and in the membranes thus depends on ambient conditions and operating parameters such as air fuel stoichiometry and operating temperature and pressure. Careful control of the governing parameters of water present in fuel cell is imperative as excess or dearth of water hampers the stack performance.

This study examines the sensitivity of the controlling parameters of water content of the overall fuel cell system. It also takes into account the effect of the non-ideal nature of some of the auxiliaries of the fuel cell system such as the air delivery sub-system and water recovery components on the controlling parameters of water balance. The limitations imposed on the design of fuel cell systems due to uneven distribution of water in the membranes or due to membrane flooding have not been considered in this study. It is assumed that the fuel cell system is capable of getting rid of the additional water that may be present throughout the membranes or in parts of it.

1.4 General Arrangement of PEM Fuel Cell and Auxiliary Systems

Figure 1-2 represents the most general arrangement of PEM fuel cell and its auxiliaries from a broad perspective without going into the specifics of each component. As shown, the hydrogen management system supplies hydrogen to the fuel cell stack. It utilizes hydrogen either directly from compressed hydrogen cylinders or from the exit of a reformer that reforms hydrocarbons like methanol. The rate at which hydrogen is consumed by the stack depends on the current drawn from it, which in turn depends on

the load requirement. The main function of the hydrogen management system is to ensure adequate supply of hydrogen to the stack and, depending upon the overall system design, re-circulate the unused hydrogen, if any, back to the stack. The supply of hydrogen is typically controlled using flow metering and regulating devices. The hydrogen management system, depending upon the stack design, also humidifies hydrogen before supplying it to the stack. Water for this purpose is supplied either by an external source or as shown in Figure 1-2 from the Water Management System.

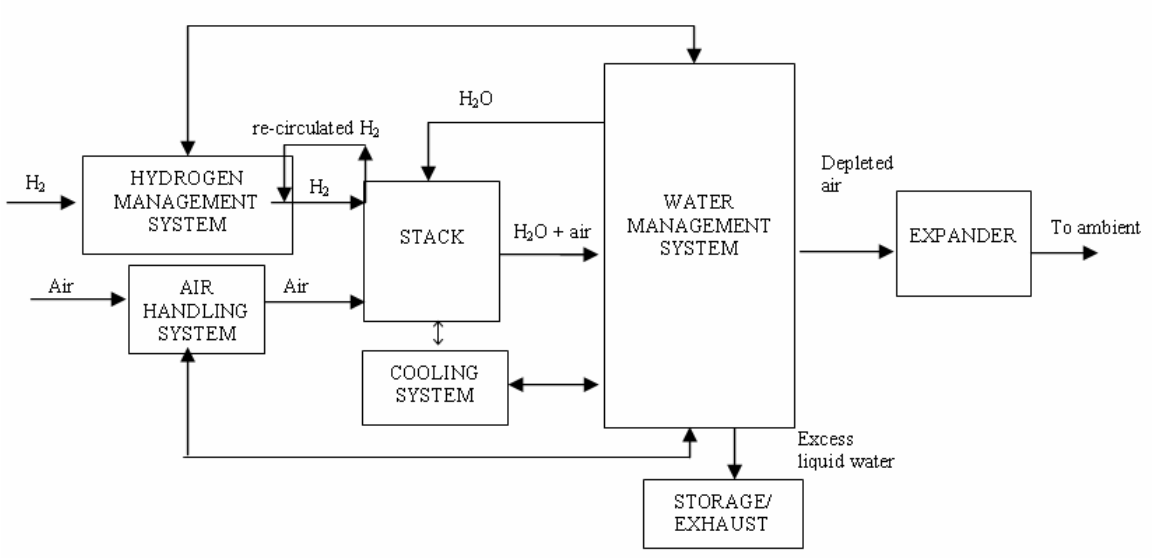

Figure 1-2. General arrangement of PEM fuel cell and auxiliaries

Figure 1-2 also shows air being supplied to the stack by the Air Handling System. The main function of the Air Handling System is to supply adequate, air for complete oxidation of hydrogen in the stack. The air, before being supplied to the stack, may be humidified, either by an external water source or with the help of the water management system. In addition, the Air Handling System may pressurize the stack. Typical equipment options for achieving this function include blowers, fans, compressors, or ejectors.

The main function of the Water Management System is to recover liquid water from the humid air leaving the stack that is depleted in oxygen, and supply part of it back to the stack to maintain the humidity of the membranes, discharging the excess or storing it. One way of achieving this function is by using a water collection device (e.g. a knockout) that separates liquid water from the depleted air leaving the stack. An alternative component is a humidity exchanger, which uses the depleted air leaving the stack to humidify the air entering the stack via a semi-permeable membrane. The membrane transfers water from its region of higher concentration (usually depleted air leaving the stack) to the region of lower concentration (usually ambient air). In a humidity exchanger, the excess water that could not be transferred to the air entering the stack is either stored or is discharged to the ambient along with the air leaving the stack. The humidified air that enters the stack via the humidity exchanger helps in maintaining the humidity of the membranes. Thus the net result of using a water separator or a humidity exchanger is the same.

A portion of the collected water, depending upon the overall design, is supplied to other auxiliaries like the Hydrogen Management System, Air Handling System and the Cooling System to aid their purpose.

The air leaving the stack is generally at higher pressure than ambient and is partially depleted of oxygen. Once water is separated from this depleted air, its pressure is reduced to ambient in an expansion device such as a valve or turbine. This device is referred to as an expander in Figure 1-2.

Lastly, the Cooling System cools the air leaving the stack and, depending upon the design choice, cools the stack itself, hence controlling the amount of water entering the

water management system in liquid form. This is typically achieved by using either a passive cooling system or a separate refrigeration device.

CHAPTER 2
LITERATURE REVIEW

This chapter reviews literature relevant to the water balance issue in PEM fuel cells. It also reviews some of the literature that, though not directly related to the water balance issue, helped in building a water balance model, which is the focus of this study.

2.1 Water Balance in PEM Fuel Cells

As mentioned earlier, the net rate at which water is generated or depleted in the fuel cell can be controlled by changing the various operating parameters like operating temperature and pressure, and air stoichiometry. Research efforts focused on improving the overall performance of the fuel cell system have also tried to determine either the mass of water present in the membranes at any point of time, or rate at which excess water is discharged from the fuel cell system.

Yu et al.[6] developed a two phase model to analyze the effect of membrane humidification on the overall performance of the stack. Air (moist or dry) and hydrogen were assumed to follow ideal gas law at all times. The flow of water through the membranes was considered as the sum of the electro-osmotic drag flux that is caused by hydrogen ion drag, diffusion flux that is caused by water concentration gradient between anode and cathode and convection flux that is caused by pressure gradient. The inputs to the model included general parameters like operating temperature and pressure and air fuel stoichiometry, and some membrane specific parameters like membrane charge concentration and membrane permeability of water. The water content in the membranes was calculated for different cases of inlet humidification and was provided as an input to

the overall model to calculate the effect on the polarization curve and stack temperature of a Ballard Mark V stack both at steady state as well as at transient conditions. The model developed to calculate the water content in the membranes, however, did not consider those operating and ambient conditions that lead to progressive loss of water from the membranes. Moreover the results of the model were specific to a particular model of fuel cell stack.

Haraldsson and Alvfors[7] used the ADVISOR software developed by National Renewable Energy Laboratory to develop an overall model for the fuel cell system. The model considered a specific arrangement of the stack and its auxiliaries that was assumed to run a mid-size automobile. The overall system included a condenser that supplied water to a storage device by condensing water from the air leaving the stack. The ADVISOR software was able to calculate the amount of water condensed at various ambient and operating conditions by using models developed for each system. The stack was assumed to be pressurized using a twin screw compressor. The study analyzed the effect of varying load conditions on water balance by calculating the change in the water quantity of the storage device when the fuel cell based automobile was assumed to run through the standard "New European Drive Cycle" (NEDC) at different altitudes and ambient temperatures. The ambient conditions were supplied as inputs to the various component models. The operating parameters were governed by the load conditions and the choice of equipment, both of which were pre-decided. The result of the analysis indicated that the quantity of water in the storage device increased over the drive cycle. This result was, however, specific to the case when a particular design of the fuel cell system and its auxiliaries was operated at the load conditions determined by NEDC. The

model did not consider continuous operation at those ambient conditions where water balance could not be achieved. Moreover it did not focus on design parameters where water balance would be achieved at all ambient conditions. Markel et al.[8] later calculated the variation in the quantity of water in the storage device for a similar arrangement of the fuel cell systems, when the fuel cell based automobile would operate at two other drive cycles, UDSS (Urban Dynamometer Driving Schedule) and US06 (the high-speed, high-acceleration-rate driving profile).The results of this model indicated that water balance was not achieved, both at cold start and hot start conditions, when the automobile operated on the US06 drive cycle. This analysis, however, like the previous one, focused on a specific arrangement of the fuel cell system. Moreover the results were specific to certain load cycle and were un-able to determine the sensitivity of various design parameters on water balance.

Stumper et al.[9] calculated the mass of water present in the membranes from the membrane ohmic resistance using known relationship between proton conductivity and water content developed by Kreuer et al.[10] The membrane resistance was calculated for known values of stack current and overall resistance offered by the fuel cell and its components, other than the membranes, like electrodes and plates. Resistance of a fuel cell was measured for a particular fuel cell system using the membrane resistance and electrode diffusivity (MRED) method, for several operating conditions. The membrane wetness calculated by this method was specific to a fuel cell stack and its internals. Moreover, the ohmic resistance of the cell internals changes over a period of time; hence its value must be periodically measured to estimate the water quantity in the membranes.

It has been seen that various studies, including the ones discussed above, that focus on the condition of the membrane, calculate either the mass of water present in the membranes at any point of time, or rate at which excess water is discharged from the fuel cell system, when particular designs of the fuel cell stack and its auxiliaries operate under specific ambient and operating conditions. None of them have made an attempt to determine the minimum system design requirements that can achieve water balance. The current study achieves this end by keeping the water balance analysis independent of the design of the fuel cell system.

2.2 Configuration of Fuel Cell Stack and Its Auxiliaries

This section contains a review of the literature on configurations of the fuel cell auxiliaries that affect water balance. Figure 2-1 shows the general arrangement of the fuel cell system considered by Haraldsson and Alvfors[7] in their analysis. The ambient air is pressurized before being supplied to the stack. In order to prevent localized dry-out and in general maintain the water content of the membranes, both the reactants, air and hydrogen, are humidified from a water reservoir before being supplied to the stack. The water reservoir also supplies water to cool the stack. Water that is used as coolant is in turn cooled by a radiator, similar to the one used in conventional automobiles. Water is supplied to the reservoir from a condenser that condenses liquid water from the air leaving the stack. The current arrangement ensures that the membranes remain moist, provided that the water reservoir always contains liquid. Gelfi et al.[12] and Cunningham[13] considered a general arrangement, similar to the one described above, for their respective studies.

Figure 2-2 shows the system configuration considered by Hussain et al.[14] The arrangement is similar to the one described above except that a separate coolant (other

than water) is used to cool the stack. The coolant in turn rejects heat to the ambient with the help of a radiator. Cooling the stack, in general, helps condense liquid water from the air leaving the stack. This condensed liquid water is used to humidify the reactants and also heat the air entering the stack.

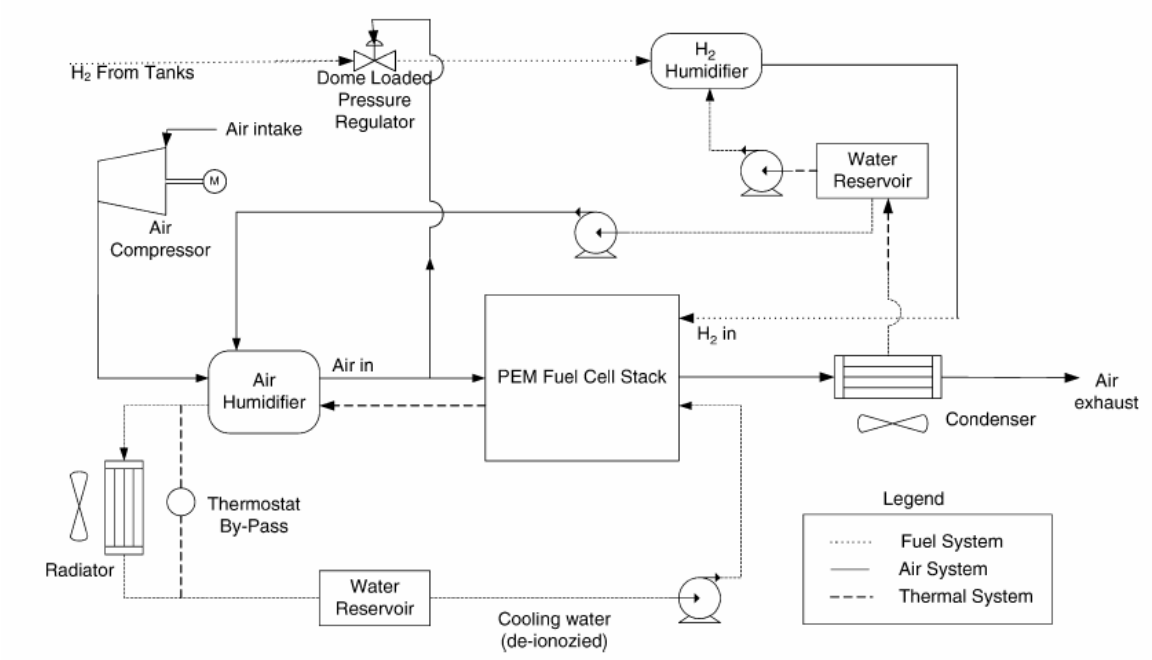

Figure 2-1 General arrangement of fuel cell systems used by Haraldsson and Alvfors[7] in their analysis

Hussain et al.[14] carried out exergy analysis of the overall system described above to predict the gross and net power developed by the fuel cell system at various ambient and operating conditions. The voltage developed by the stack was predicted using the model developed by Baschuk and Li.[15]

The 1.2 kW Nexa® fuel cell system developed by Ballard systems does not use a pressurized stack. Water recovery from the air leaving the stack is achieved by a humidity exchanger instead of a condenser or water separator. A humidity exchanger uses a semi-permeable membrane to transfer water from its region of higher

concentration (usually depleted air leaving the stack) to the region of lower concentration (usually ambient air). The ambient air, in turn, helps in maintaining the water content of the membranes.

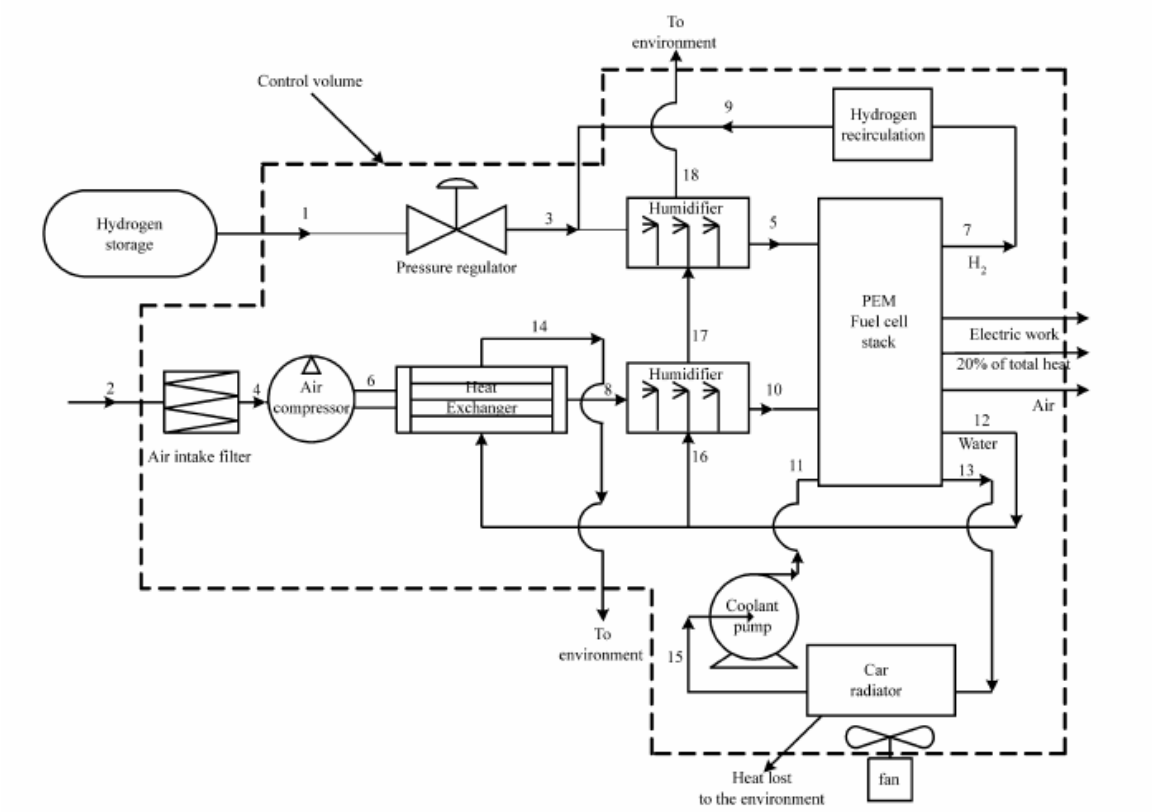

Figure 2-2 General arrangement of fuel cell systems used by Hussain et al.[14] in their analysis

A change in the operating pressure of the fuel cell stack varies the saturation pressure of the moist air leaving the stack. The saturation pressure of the exhaust air determines the rate at which liquid water leaves the fuel cell and affects the water balance of the overall system. Thus a change in operating pressure of the stack affects the water balance of the fuel cell system. The pressure ratio (or the operating pressure of the stack) and the power consumption of a pressurizer vary with the change in load conditions. As these performance characteristics vary with the type and model of equipment, selection of

the pressurization equipment is critical to the overall performance of the fuel cell in general and water balance in particular.

Kulp[16] compared the effect of using a centrifugal compressor as opposed to a twin screw compressor, on the performance of a 60 kW PEM fuel cell stack. Actual compressor maps were used to model the performance of each compression device under varying operating conditions. A specific voltage equation that relates stack voltage to current density, average stack temperature and average partial pressure of oxygen in the stack was used to develop polarization curves of the stack. The study concluded that the centrifugal compressor is more efficient than the screw compressor when a expander (a turbine that supplies power to the compressor) is used in conjunction with the compression device.

Cunningham[13] used the performance characteristics of an Allied Signal centrifugal compressor to develop a model for simulating the performance of the air supply system used in fuel cell vehicle. The compressor map of an Allied Signal compressor was also used by Peng et al.[17] to develop a control oriented model of the fuel cell system. The stack was modeled using polarization data of 75 kW fuel cell stack. The fuel cell auxiliaries other than the compressor were modeled using conservation laws. The current study also uses the performance characteristics of the same Allied Signal compressor model to demonstrate the effect of using a non-ideal compressor on water balance.

2.3 Different Models to Predict Properties of Moist Air at Elevated Temperature and Pressure

The air leaving the stack is generally at an elevated temperature and pressure and is partially depleted of oxygen. Ji et al.[18] compared the properties of moist air calculated from different models with the experimental data. The results of this analysis concluded

that the accuracy of the ideal gas model decreases with the increase in pressure. Thus the ideal gas law is not accurate enough to calculate the properties of moist air leaving a high pressure stack and real gas models have to be used.

The real gas models studied by Ji et al.[18] included the ideal mixing model that considered moist air as an ideal mixture of two real gases, vapor and dry air. This model was found accurate enough to calculate the properties of saturated vapor at pressures less than 10 bar and temperatures above 280 K. Other real gas models studied by Ji et al. are

- The model developed by Luks et al.[18] that is accurate in a temperature range of 200 K to 600 K for pressures as high as 200 atmospheres.
- Hyland and Wexler model[18] accurate in temperature range of 173.15 K to 473.15 K for pressures as high as 50 atmospheres.
- Model of Rabinovich and Beketov[18] which is accurate to a temperature of 400K and a pressure of 100 atmospheres.

The results of the study determined the Hyland and Wexler model to be more accurate than the other models. Each of the above-mentioned models is based on the virial equation of real gases and aims towards calculating the virial coefficients and cross virial coefficients of the air vapor mixture. The equation of state developed by each of these models are applicable to standard air having a composition of 21% oxygen and is not applicable to moist air depleted in oxygen.

Xiaoyan and Jinyue[19] used the ideal mixing model to calculate the properties of saturated moist air. Air and vapor were assumed to follow the modified Redlich-Kwong equation. Henry's Law was used to calculate the mole fraction of vapor in moist air. One of the inputs to the model was the total number of moles of moist air. This limited the

model to calculate the properties of moist air flow only when its molar flow rate or total number of moles was known.

When the quantity of moist air is unknown, the mole fraction of vapor in moist air can be calculated by using the ideal mixing model in conjunction with the Poynting effect.[20] This approach has followed in the current study to estimate the properties of depleted and pressurized moist air leaving the stack.

CHAPTER 3
WATER BALANCE MODEL

To analyze the effect of various operating parameters on the water balance of PEM fuel cells, a control volume analysis was carried out for steady state operation of the fuel cell system. As a part of the analysis, a control volume was defined for the most general arrangement of PEM fuel cell systems. As shown in Figure 3-1, the fuel cell stack and various systems, except the expander and storage device, are inside the control volume.

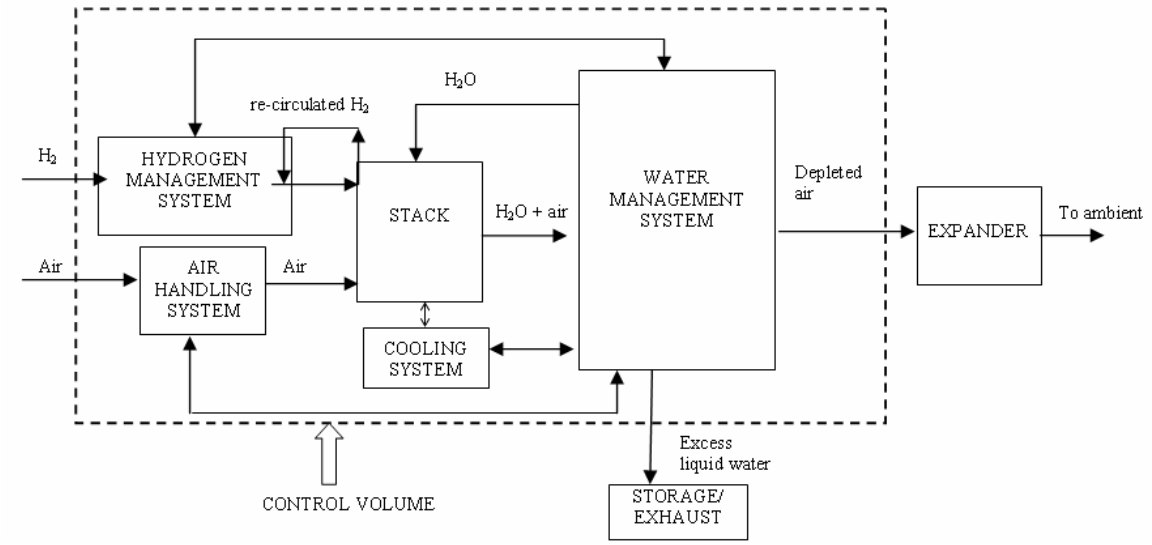

Figure 3-1. Control volume defined for the general arrangement of PEM fuel cell and auxiliary systems

Water enters the control volume in vapor state as a part of the atmospheric air at a mass flow rate of $\dot{m}_{H_2O\text{-}in}$. Water is generated inside the fuel cell (and hence the control volume) as a result of the electro-chemical reaction where hydrogen reacts with oxygen present in the ambient air to form water. In this study, it is assumed that the net hydrogen (hydrogen supplied – hydrogen re-circulated) entering the stack (and hence the control

volume) is completely converted to water by supplying adequate air to facilitate the reaction. The net rate at which hydrogen enters the control volume depends on the current drawn from the stack, which in turn varies with the varying load requirement. Hence, the mass rate of water generation $\dot{m}_{H_2O\text{-}gen}$ is a function of the current drawn from the stack. A portion of $\dot{m}_{H_2O\text{-}gen}$, depending upon the ambient and operating conditions, is entrained along with the air that leaves the stack.

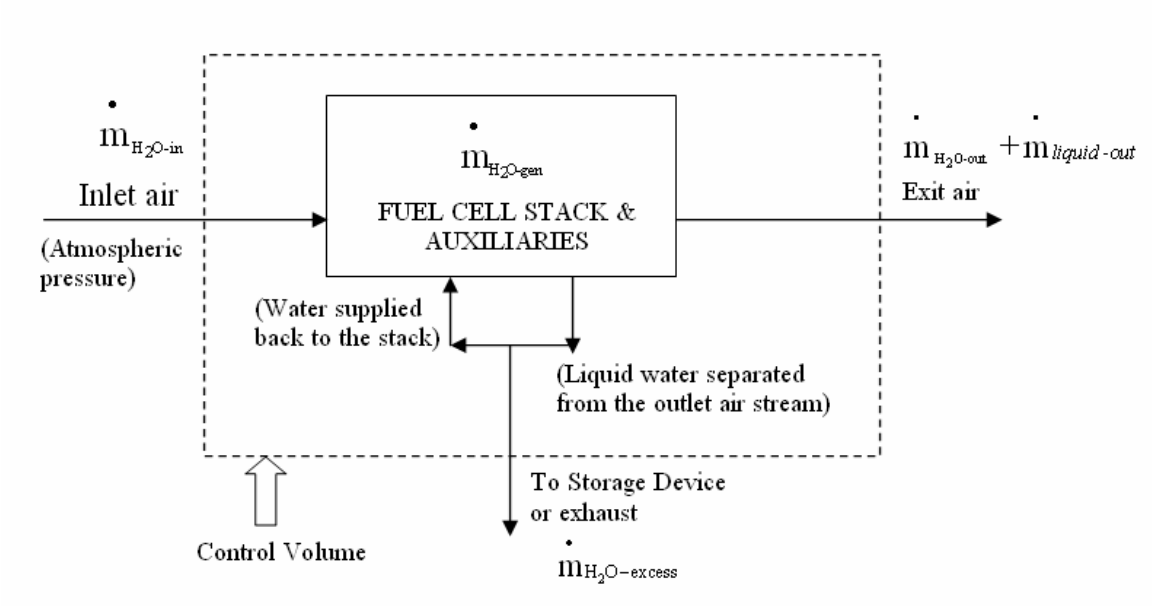

Figure 3-2. Different flow streams of water crossing the control volume boundary

The water collection/separation device separates liquid water, if any, carried along with the air leaving the stack. Part of this liquid water is supplied back to the stack to maintain the humidity of the membranes. The remaining portion (referred to as excess water) leaves the control volume at a mass flow rate of $\dot{m}_{H_2O\text{-}excess}$ and is either discharged to the ambient or stored in a storage device.

Water leaves the control volume in the form of vapor, at the rate of $\dot{m}_{H_2O\text{-out}}$, as a part of the air depleted in oxygen (referred to as depleted air) that leaves the control volume after exiting the stack and other components such as a water separator. The air leaving the control volume also carries along with it a portion of the liquid water, which could not be separated in the water separator/collector, at a mass flow rate of $\dot{m}_{liquid-out}$.

For the current analysis, the control volume is assumed to be in steady state at all conditions. Water needs to be constantly supplied to the membranes to maintain their humidity level. From a global standpoint, the water used to humidify the membranes can only originate from the hydrogen oxidation reaction or from humidity in the inlet air. Hence, steady operation requires that the sum of those two sources be greater than the rate at which water is lost as a part of the exhaust, both in liquid and vapor form. Thus the mass flow rate of excess water should be greater than zero to achieve water balance at steady state and prevent membranes from progressively drying out.

In order to determine the effect of various operating parameters on water balance, an expression for the mass flow rate of excess water is required in terms of ambient and design parameters. This expression would help in calculating the mass flow rate of excess water for known values of operating conditions, which in turn would determine whether water balance is achieved under those conditions. The sensitivity of the controlling parameters of water balance could also be determined from this expression.

3.1 Expression for the Mass Flow Rate of Excess Water

The integral form of continuity equation for water inside the control volume is

$$\frac{\partial}{\partial t}\int_{CV}\rho_{H_2O}dV+\int_{CS}\rho_{H_2O}(\vec{v}\cdot\overrightarrow{dA})=\dot{m}_{H_2O\text{-gen}} \qquad 3\text{-}1$$

where $\frac{\partial}{\partial t}\int_{CV}\rho_{H_2O}dV$ represents the rate of change of mass of water inside the control volume, $\int_{CS}\rho_{H_2O}(\vec{v}\cdot\vec{dA})$ represents the net rate at which water leaves the control volume and $\dot{m}_{H_2O-gen}$ represents the rate at which mass is generated inside the control volume. As the control volume is at steady state, the first term is zero. The second term, based on the control volume shown in Figure 3-2, is

$$\int_{CS}\rho_{H_2O}(\vec{v}\cdot\vec{dA}) = \dot{m}_{H_2O-out} + \dot{m}_{liquid-out} + \dot{m}_{H_2O-excess} - \dot{m}_{H_2O-in} \qquad 3\text{-}2$$

The third term, the net rate at which water is generated inside the control volume, is $\dot{m}_{H_2O-gen}$. Thus Equation 3-1 can we written as

$$\dot{m}_{H_2O-excess} = \dot{m}_{H_2O-in} + \dot{m}_{H_2O-gen} - \dot{m}_{H_2O-out} - \dot{m}_{liquid-out} \qquad 3\text{-}3$$

As explained earlier, when the value of $\dot{m}_{H_2O-excess}$ is negative, the membranes will eventually dry out.

The next step is to express the variables on the right hand side of Equation 3-3 in terms of ambient conditions and design parameters of the fuel cell. The mass flow rate at which water vapor enters the control volume as a part of ambient air, $\dot{m}_{H_2O-in}$, depends on the mass flow rate of ambient air supplied to the fuel cell which in turn depends on the requirement of oxygen for the electrochemical reaction. The overall reaction inside the fuel cell is as follows:

$$H_2 + \frac{1}{2}O_2 \Rightarrow H_2O \qquad 3\text{-}4$$

Each mole of diatomic hydrogen (H_2) supplied requires half a mole of oxygen (O_2) to form one mole of water.

Let N_{H_2} be the molar flow rate of diatomic hydrogen entering the control volume. For full utilization of the fuel, the minimum required molar flow rate of oxygen is $N_{H_2}/2$. If y is the fraction of excess air supplied, then the actual molar flow rate of oxygen is $(1+y)\, N_{H_2}/2$.

If $\chi_{O2\text{-dry}}$ is the mole fraction of oxygen in dry ambient air (often assumed to be 0.21) then the molar flow rate of dry ambient air entering the control volume is

$$\frac{(1+y)N_{H_2}}{2\chi_{O_2-\text{dry}}}$$

Thus, the mass flow rate of water entering the control volume along with ambient air in vapor form is

$$\dot{m}_{H_2O-in} = \frac{M_w \chi_{H_2O\text{-in}} (1+y)N_{H_2}}{2\chi_{O_2-\text{dry}}(1-\chi_{H_2O\text{-in}})} \qquad 3\text{-}5$$

where $\chi_{H_2O\text{-in}}$ is the mole fraction of water in the ambient air and M_w is the molecular weight of water.

The molar rate of oxygen consumption inside the fuel cell is $N_{H_2}/2$ (assuming complete conversion of hydrogen to water). Hence the molar flow rate of dry depleted air leaving the control volume is

$$\frac{(1+y-\chi_{O_2-\text{dry}})N_{H_2}}{2\chi_{O_2-\text{dry}}}$$

and the mass flow rate of water leaving the control volume ($\dot{m}_{H_2O-out}$) is

$$\dot{m}_{H_2O-out} = \frac{M_w \chi_{H_2O\text{-}out}(1+y-\chi_{O_2-dry})N_{H_2}}{2\chi_{O_2-dry}(1-\chi_{H_2O\text{-}out})} \quad 3\text{-}6$$

where $\chi_{H_2O\text{-}out}$ is the mole fraction of water in the depleted air.

As can be seen from Equation 3-4, for each mole of diatomic hydrogen utilized one mole of water is produced. Thus the molar rate of water generation inside the control volume is N_{H_2} and the mass rate of water production is

$$\dot{m}_{H_2O-gen} = M_w \,.\, N_{H_2} \quad 3\text{-}7$$

Substituting the expressions derived in Equations 3-5, 3-6 and 3-7 in Equation 3-3, we find the mass flow rate of excess water produced as

$$\dot{m}_{H_2O-excess} = M_w \left\{ N_{H_2} + \left[\frac{\chi_{H_2O\text{-}in}(1+y)N_{H_2}}{2\chi_{O_2-dry}(1-\chi_{H_2O\text{-}in})} \right] - \left[\frac{\chi_{H_2O\text{-}out}(1+y-\chi_{O_2})N_{H_2}}{2\chi_{O_2-dry}(1-\chi_{H_2O\text{-}out})} \right] \right\} - \dot{m}_{liquid-out} \quad 3\text{-}8$$

The mass flow rate of excess water was expressed in non-dimensional terms by dividing Equation 3-8 by the mass rate of water produced ($\dot{m}_{H_2O-gen}$)

$$M'_{excess} = 1 + \left[\frac{\chi_{H_2O\text{-}in}(1+y)}{2\chi_{O_2-dry}(1-\chi_{H_2O\text{-}in})} \right] - \left[\frac{\chi_{H_2O\text{-}out}(1+y-\chi_{O_2})}{2\chi_{O_2-dry}(1-\chi_{H_2O\text{-}out})} \right] - \left[\dot{m}_{liquid-out} / \dot{m}_{H_2O-gen} \right] \quad 3\text{-}9$$

Here, M'_{excess} is the non-dimensional form of the excess water rate and is equal to the mass flow rate of excess water per unit mass rate of water produced. The term $\dot{m}_{liquid-out} / \dot{m}_{H_2O-gen}$ represents the non-dimensional form of the mass flow rate of liquid water carried along with the depleted air as it could not be separated or recovered. This term

shall be represented by variable $M'_{liquid-out}$ and shall be referred to as non-dimensional un-recovered liquid water.

As explained earlier, when the value of $\dot{m}_{H_2O-excess}$ is negative, the membranes will dry out eventually. It can be seen from Equations 3-8 and 3-9 a non-negative $\dot{m}_{H_2O-excess}$ would mean a non-negative value of M'_{excess}, as $\dot{m}_{H_2O-gen}$ is always positive. Hence in order to achieve water balance under steady state conditions and prevent the membranes from drying out, the value of the non-dimensional term M'_{excess} should be always positive. The next section explains the procedure to calculate the value of M'_{excess} in order to determine whether water balance is achieved at steady state for a particular set of ambient and operating conditions.

3.2 Procedure to Calculate M'_{excess}

Based on Equation 3-9, the inputs required to calculate the value of M'_{excess} are $\chi_{H_2O\text{-in}}$, χ_{O_2-dry}, $\chi_{H_2O\text{-out}}$, y and $M'_{liquid-out}$. Of these variables, $\chi_{H_2O\text{-in}}$ and χ_{O_2-dry} govern the amount of water and oxygen present in the ambient air respectively and their values depend on the ambient conditions. The other variables, $\chi_{H_2O\text{-out}}$, $M'_{liquid-out}$ and y, are independent, and their values depend on the design conditions. Thus the value of M'_{excess} can be calculated at different ambient conditions and design choices. A Matlab® code was developed that would calculate the value of M'_{excess} for various inputs.

The value of χ_{O_2-dry} was assumed to be 0.21 in the current analysis. For all terrestrial conditions, the properties of humid ambient air can be accurately calculated

using the ideal gas law.[18] Thus ambient air at the inlet to the control volume was modeled using the ideal gas law. Given this, $\chi_{H_2O\text{-in}}$ can be equated to the ratio of partial pressure of water vapor to the total pressure i.e.

$$\chi_{H_2O\text{-in}} = \frac{\phi . p_s}{p_{amb}} \qquad 3\text{-}10$$

Here, the relative humidity of ambient air ϕ and the ambient pressure p_{amb} depend on the atmospheric conditions and are inputs to the model. The saturation pressure of the vapor in the ambient air, p_s was calculated using the Hyland and Wexler[18] equation for saturated vapor pressure which is given as follows:

$$\log(p_s) = (-0.58002206x10^4/T_a) + 1.3914993 - (0.048640239.T_a) + (0.41764768x10^{-4}.T_a^2) - (0.14452093x10^{-7}.T_a^3) + (6.5459673.\log(T_a)) \qquad 3\text{-}11$$

The ambient temperature T_a was an input to the model. The ambient air properties, namely pressure, temperature and relative humidity, define the humidity ratio of the ambient air, which governs the amount of water entering the control volume. However, ambient conditions are not commonly expressed in terms of its humidity ratio. Hence pressure, temperature and relative humidity, which more commonly represent the ambient air conditions, are used as inputs to the model. Any combination of the three inputs that give rise to a particular value of humidity ratio will give the same result.

In order to calculate $\chi_{H_2O\text{-out}}$, the properties of depleted air must be known. In the current model, it is assumed that depleted air leaving the control volume is saturated. Depleted air is usually at an elevated pressure and temperature. At explained earlier in Chapter 2, the accuracy of the ideal gas model decreases with increasing pressure. For the

flow leaving the control volume, the current model uses the Redlich-Kwong (RK)[20] equation for real gases for each of its constituents:

$$p_{real} = \frac{RT_{real}}{(\nu_{real} - b)} - \frac{a}{\nu_{real}(\nu_{real} + b)T_{real}^{0.5}} \qquad 3\text{-}12$$

where p_{real} is the pressure of a real gas, T_{real} is its temperature and ν_{real} its molar volume in. The symbols a, b and R are represent constants where R is the universal gas constant

$$a = 0.42748\ \frac{R^2 T_c^{2.5}}{P_c} \quad \text{and} \quad b = 0.08664\ \frac{RT_c}{P_c} \qquad 3\text{-}13$$

T_c and P_c are the critical temperature and critical pressure, respectively, of the real gas.

Xiaoyan and Jinyue[19] used the Redlich-Kwong equation to model the properties of pure vapor, nitrogen, oxygen and a mixture of all three gases for different mole fractions of each component. The results of the model were compared with experimental data and the accuracy of the model was found to be in the range of ±0.45%. Thus the Redlich-Kwong equation is considered sufficiently accurate to calculate the properties of depleted air.

In order to calculate the properties of the vapor in depleted air, the temperature and pressure of depleted air must be supplied to the model as an input.

Let p_t be the pressure of the depleted air at the exit of the control volume and p_r (compression ratio) be the ratio of depleted air pressure to ambient pressure. Thus

$$p_r = p_t / p_{amb} \qquad 3\text{-}14$$

The saturation pressure of vapor in the depleted air is different than the saturation pressure of pure vapor at the same temperature due to the presence of non-condensable dry air along with the vapor. In order to calculate the saturation pressure of the vapor in the depleted air, the Poynting effect[20] was considered. Following the Poynting effect,

pure water vapor is assumed to be in equilibrium with liquid water at the depleted air temperature. State 1 be the state of the water vapor and liquid water mixture at the depleted air temperature. The pressure of the vapor and the liquid at State 1 would thus be equal to the saturation pressure corresponding to the depleted air temperature. Dry air was now assumed to be added to the pure vapor at constant temperature until the total pressure of the air-vapor mixture equals the depleted air pressure, p_t. This would modify the partial pressure of vapor which is still in the saturated condition. State 2 be the state of the moist air and liquid water mixture after addition of non-condensable gases to water vapor. The pressure of the liquid water at State 2, which is in equilibrium with the air vapor mixture above it, would be equal to the depleted air pressure. The modified saturation vapor pressure is calculated by equating the change in Gibbs free energy at the liquid-vapor interface from State 1 to 2 when an infinitesimal quantity of non condensable gases is added to a pure liquid vapor mixture at a constant temperature. This gives the following equation:

$$dg_{liquid} = dg_{vapor} \qquad 3\text{-}15$$

where g_{liquid} and g_{vapor} are the gibbs free energies of liquid and vapor respectively. As the temperature of liquid and vapor does not change between State 1 and 2, $dg = \upsilon.dp$

Thus Equation 3-15 can be written as

$$(\nu\, dp)_{liquid} = (\nu\, dp)_{vapor} \qquad 3\text{-}16$$

Integrating between State 1 and 2, to calculate the total change in the gibbs free energy at the liquid-vapor interface, the following equation is obtained.

$$\int_{p_1}^{p_2} \nu dp = (p_2.\nu_2) - (p_1.\ \nu_1) - \int_{\nu_1}^{\nu_2} p d\nu = \nu_{liq}(p_t - p_1) \qquad 3\text{-}17$$

Here p_2 represents the modified saturation pressure of the vapor at State 2, when the total pressure of the air-vapor mixture is p_t (depleted air pressure). The molar volume of liquid water, ν_{liq}, is assumed approximately constant between State 1 and 2, and its value is taken as 18.016×10^{-6} m^3/mole.

As mentioned earlier the temperature T_1 (temperature of the depleted air) is an input to the model. The saturation pressure of pure vapor at the depleted air temperature (p_1) is calculated at temperature T_1 using the Hyland and Wexler equation. The molar volume of vapor at State 1 (ν_1) is calculated by the R.K. equation with p_1 as the input. The modified saturation pressure (p_2) is expressed in terms of ν_2 using the R.K. equation and $\int_{\nu_1}^{\nu_2} p d\nu$ is also expressed in terms of ν_2, as ν_1 is known. As a result, Equation 3-17 takes the form

$$\frac{RT.\nu_2}{(\nu_2 - b)} - \frac{a}{(\nu_2 + b)T^{0.5}} - (p_1.\ \nu_1) - RT.\ln\left[\frac{(\nu_2 - b)}{(\nu_1 - b)}\right] - \left(\frac{a}{bT^{0.5}}\right)\ln\left[\frac{\nu_1(\nu_2 + b)}{\nu_2(\nu_1 + b)}\right] = (18.016 \times 10^{-6})(p_t - p_1) \qquad 3\text{-}18$$

Except for ν_2 and p_t all other variable in the above equation are known. The depleted air pressure p_t is one of the parameters that is varied in order to observe its effect on the excess water produced and is hence an input to the equation.

For a particular value of p_t, ν_2 is calculated iteratively by the code. The value of ν_2 is used to find the value of p_2 (modified saturation pressure of vapor in the depleted air) using the RK equation.

For developing the model, the mixture of dry air and vapor is considered to be an ideal solution. Hence, the mole fraction of vapor in depleted air $\chi_{H_2O\text{-}out}$ is equal to the

ratio of the fugacity of the vapor at its partial pressure to the fugacity of the vapor at the total pressure of the mixture,[20] or

$$\chi_{H_2O\text{-out}} = \frac{f(p_2, T_1)}{f(p_t, T_1)} \qquad 3\text{-}19$$

In Equation 3-19, $f(p_2,T_1)$ is the fugacity of vapor at pressure p_2 and temperature T_1 and $f(p_t,T_1)$ is the fugacity at pressure p_t and temperature T_1. Fugacity of a gas that follows Redlich-Kwong equation is given by[20]

$$f = \exp\left\{\frac{b}{(v-b)} + \ln\left[\frac{RT}{(v-b)}\right] - \frac{a}{RT^{1.5}}\left(\frac{1}{(v+b)} + \frac{1}{b}\ln\left[\frac{v+b}{v}\right]\right)\right\} \qquad 3\text{-}20$$

Equation 3-20 is used to calculate the value of $f(p_2,T_1)$, as v_2 and T_1 are already known. The value of p_t is input in the R.K. equation to determine the value of v_t and the value of $f(p_t,T_1)$ is determined using Equation 3-20. Consequently, $\chi_{H_2O\text{-out}}$ can be calculated for different values of p_t at a given value of T_1. From Equations 3-9, 3-10, and 3-19, M'_{excess} can be calculated when ambient temperature (T_a), ambient pressure (p_{amb}), ambient relative humidity (Φ), fraction of excess air (y), depleted air temperature (T_1), $M'_{liquid-out}$ and depleted air pressure (p_t) are provided as input. Of these inputs, y, T_1, $M'_{liquid-out}$ and p_t are design parameters, as their values can be varied using different equipment choices and operating conditions.

3.3 Model Validation

In order to validate the accuracy of the water balance model developed above, the results of the model were compared with the values calculated by the Hyland and Wexler[18] model, which has been accepted to be more accurate in comparison to other real gas models for moist air.[18] As the Hyland and Wexler model was not applicable for

depleted air, the water balance model was used to calculate the humidity ratio (ω) of ambient air and its values were compared with those calculated by the Hyland and Wexler model for different ambient temperatures and pressures. Tables 3-1 and 3-2 show the comparison of different values of ω at sea level and 2250 meters. Figure 3-3 graphically represents the deviation of the values calculated using the model from the readings calculated by the Hyland and Wexler model. It can be seen that the current model based on R.K. equation, closely follows the Hyland and Wexler model and the deviation in the value of ω for different temperatures at two different elevations is less than ±5%.

Table 3-1. Comparison of different values of ω at sea level

Sea level: 101.325 kPa				
Temperature (°C)	% RH	ω (humidity ratio)		Percent error
		Hyland and Wexler model	Current model based on RK equation	Current model v/s Hyland and Wexler readings
5	100	0.0054	0.0055	-1.59%
10	100	0.0076	0.0077	-1.15%
15	100	0.0107	0.0107	-0.28%
20	100	0.0147	0.0147	0.38%
25	100	0.0202	0.0199	1.42%
30	100	0.0273	0.0266	2.73%

Table 3-2. Comparison of different values of ω at 2250 meters

Altitude 2250 meters : 77.058 kPa				
Temperature (°C)	% RH	ω (humidity ratio)		Percent error
		Hyland and Wexler model	Current model based on RK equation	Current model v/s Hyland and Wexler readings
5	100	0.0072	0.0072	-0.16%
10	100	0.0102	0.0101	0.89%
15	100	0.0142	0.014	1.24%
20	100	0.0195	0.0192	1.50%
25	100	0.027	0.026	3.69%
27	100	0.0303	0.0293	3.60%

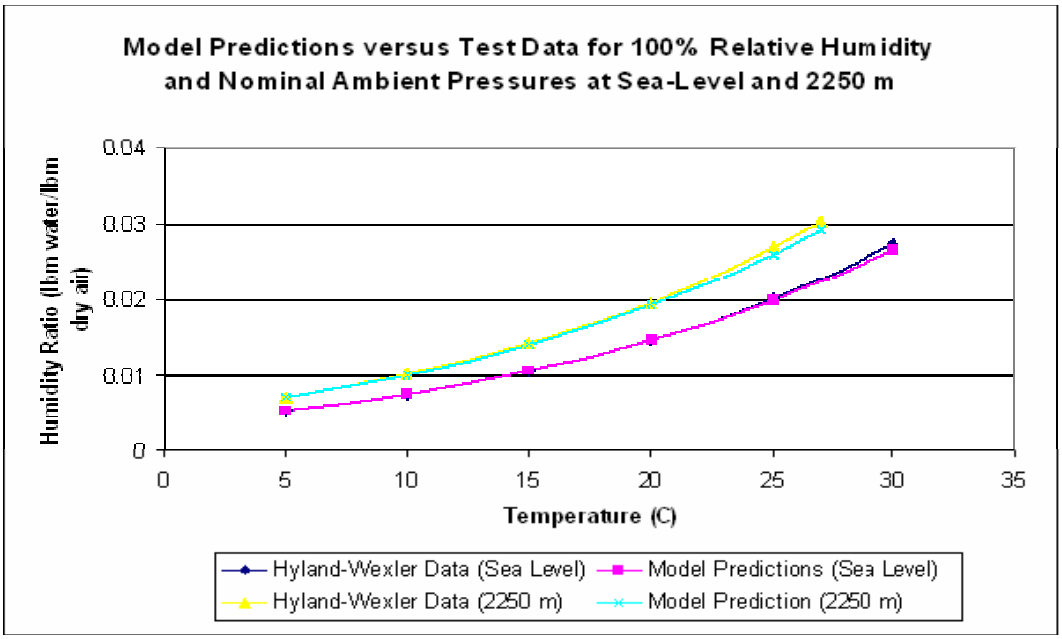

Figure 3-3. Comparison of model predictions with Hyland and Wexler data

CHAPTER 4
RESULTS AND DISCUSSION

In order to achieve water balance at steady state, the value of the non-dimensional excess water term M'_{excess} should be greater than zero. As seen previously in Chapter 3, the dimensionless form of excess water M'_{excess} can be calculated when ambient temperature, pressure and relative humidity and design parameters pressure ratio, depleted air temperature, non-dimensional form of un-recovered liquid water $M'_{liquid-out}$ and fraction of excess air are provided as inputs. Of these inputs, the ones that can be controlled are only the design parameters.

The ambient conditions and stoichiometry govern the amount of water entering the control volume. For a given set of operating conditions, any increase in the humidity ratio of the ambient air would bring more water into the control volume and hence would increase the value of M'_{excess}. This can also be seen from Equation 3-9 in which an increase in $\chi_{H_2O\text{-in}}$ (the mole fraction of water in ambient air) increases the value of M'_{excess}. As ambient conditions cannot be controlled, the fuel cell must be designed for the worst operating conditions which, from a water balance point of view, would be ambient air with a relative humidity of zero. At completely dry ambient conditions, i.e., at Φ=0, $\chi_{H_2O\text{-in}}$ is zero for all ambient temperatures. Hence M'_{excess} is independent of ambient temperature at Φ=0.

In addition to being able to operate under dry ambient conditions, fuel cell-driven vehicles should be capable of operating at high altitudes (low ambient pressure). To consider the effect of low ambient pressure on water balance, a maximum altitude limit of 12,000 feet that corresponds to 64.539 kPa was considered in this study. An altitude of 12,000 feet is the more commonly accepted upper limit for high altitudes that is used by fuel cell automobile manufacturers.

To analyze the variation of M'_{excess} for dry ambient conditions (Φ=0), the Matlab® code was used to plot 3D graphs of M'_{excess} versus y and p_r at different depleted air temperatures and altitudes. For the initial part of the analysis, the value of $M'_{liquid-out}$ was chosen to be zero.

Figures 4-1 to 4-4 are the plots showing variation of M'_{excess} at four different depleted air temperatures at an ambient pressure of 101.325 kPa. Figures 4-5 to 4-8 are similar to Figures 4-1 to 4-4 except that the ambient pressure is 64.539 kPa, corresponding to an altitude of 12,000 feet, in all of these cases.

Figures 4-1 to 4-8 indicate that for a given excess air fraction y, M'_{excess} increases with the increase in pressure ratio. An increase in depleted air pressure for a given depleted air temperature decreases the humidity ratio of the depleted air and causes more water to condense. Hence less water leaves the control volume as a part of the depleted air and the excess water variable increases. This trend is seen at all ambient conditions. Mathematically, an increase in depleted air pressure decreases the humidity ratio of depleted air and hence the value of $\chi_{H_2O\text{-out}}$. This in turn decreases the value of $[\chi_{H_2O\text{-out}}(1+y-\chi o_2)/2\,\chi o_2(1-\chi_{H_2O\text{-out}})]$ and increases the value of M'_{excess} based on Equation 3-9. This is the same as mentioned before.

A comparison of the values of M'_{excess} at different depleted air temperatures, in Figures 4-1 through 4-4 for sea level and Figures 4-5 through 4-8 for 12,000 feet, shows that a decrease in the depleted air temperature increases the value of M'_{excess}. A decrease in the depleted air temperature when all other parameters are kept constant, decreases the humidity ratio of the depleted air and causes more water to condense. Hence less water leaves the control volume as a part of the depleted air and the excess water variable increases. This trend is consistent under all ambient conditions.

An increase in the quantity of excess air for a given depleted air pressure decreases the value of M'_{excess} for the ambient conditions under consideration. The incoming or ambient air is dry and takes in part of the water generated in the fuel cell to become saturated. An increase in the fraction of excess air increases the mass flow rate of the ambient air for a given water production rate. Thus more water is required to saturate the incoming air, which in turn implies that a greater portion of the water generated leaves the control volume as a part of the depleted air than as excess water. Consequently the rate of excess water produced decreases. This trend, however, is specific to the ambient conditions under consideration and changes completely for humid ambient cases.

It can be seen from Equation 3-9 that a change in the value of $M'_{liquid-out}$ results in an equal change in the value of M'_{excess}. The shape of a plot of M'_{excess} versus any of the controlling parameters, for a constant $M'_{liquid-out}$, remains unaltered for all values of $M'_{liquid-out}$. This effect is indicated in Figure 4-11, showing M'_{excess} versus pressure ratio for $M'_{liquid-out}$=0 and $M'_{liquid-out}$=0.1. The ambient temperature, pressure and relative humidity were assumed to be 298 K, 1 atmosphere and 0%, respectively, and the depleted air

temperature was assumed to be 353 K. The values of $M'_{liquid-out}$ were assumed to stay constant at 0 and 0.1 with the change in pressure, for both cases.

It can be seen from Figure 4-11 that the trend of variation of M'_{excess} does not change with a variation in the value of $M'_{liquid-out}$. The only effect, as mentioned before, is a drop in the value of M'_{excess} by an amount equal to $M'_{liquid-out}$. An implication of this effect is that if M'_{excess} is negative (water balance not achieved at steady state) for $M'_{liquid-out}$=0 under certain operating conditions, water balance will never be achieved at those conditions for all positive values of $M'_{liquid-out}$. Thus analyzing the case of $M'_{liquid-out}$=0 determines those values of design parameters where water balance cannot be achieved for all values of $M'_{liquid-out}$. It should be noted that the value $M'_{liquid-out}$ cannot be less than zero as it is the non-dimensional form of the amount of liquid water that could not be separated from depleted air.

It can be seen from Figures 4-1, 4-2, 4-5 and 4-6 that, when operating at sea level and even at 12000 feet, a depleted air temperature of 298K would produce excess water even when the fraction of excess air is as high as 4, for $M'_{liquid-out}$=0. A value of $M'_{liquid-out}$>0.75 would drop M'_{excess} below zero and pressurization may be needed in those cases to achieve water balance. In general, pressurization of the fuel cell is not required even at 12,000 feet for a maximum value of *y* as high as 4 when $M'_{liquid-out}$<0.75. However, depleted air temperatures as low as 298K for a fuel cell that operates close to 353K is possible only when a refrigeration system cools the stack.

Figure 4-3 shows that when the depleted air temperature is increased to 323K at sea level, water balance is not achieved at $M'_{liquid-out}$=0 for an un-pressurized stack when the

fraction of excess air *y* increases beyond 2 . In such cases, the fuel cell must be pressured for all values of $M'_{liquid-out}$, to prevent membrane dry-out under continuous operation. An increase in altitude to 12000 feet at a depleted air temperature of 323K drastically affects the water balance as the system must be pressurized for excess air fraction beyond 1.

When the depleted air temperatures are as high as 353K, the fuel cell must be pressured under all operating conditions to ensure production of excess water. Moreover at 12000 feet, excess water is produced only at very high depleted air pressures and low excess air fractions. Such operating conditions place significant constraints on system design.

Figures 4-1 to 4-4 for sea level and Figures 4-5 to 4-8 for an altitude of 12,000 feet indicate that an increase in depleted air temperature moves the constant excess air lines on the M'_{excess} versus pressure ratio plot closer to each other. This can be seen from Equation 3-9. As ambient relative humidity is zero, $\chi_{H_2O\text{-in}}$ =0 hence Equation 3-9 becomes

$$M'_{excess} = 1 - \left[\frac{\chi_{H_2O\text{-out}}(1+y-\chi_{O_2})}{2\chi_{O_2}(1-\chi_{H_2O\text{-out}})} \right] + M'_{liquid-out}$$

An increase in depleted air temperature at dry ambient conditions increases the saturation pressure of depleted air. Hence $\chi_{H_2O\text{-out}}$ increases and $\chi_{H_2O\text{-out}}/(1-\chi_{H_2O\text{-out}})$ decreases. As this term is the multiplying factor to the term $(1+y-\chi o_2)$, any increase in *y* has a comparatively lesser impact on M'_{excess} for higher depleted air temperatures than for lower ones. Thus the constant excess air lines move closer to each other for higher temperatures

at dry ambient conditions. As explained earlier, this trend would stay the same for all values of $M'_{liquid-out}$.

So far we have observed the trend of variation of M'_{excess} with respect to excess air y for dry ambient conditions. The trend is not always same when the ambient air has a relative humidity greater than zero. Figure 4-9 is again a plot of M'_{excess} with operating conditions the same as those in Figure 4-2 except that the relative humidity, Φ is 0.5 instead of zero. Comparing Figure 4-2 with Figure 4-9 shows that the excess water produced at particular operating and ambient conditions is always greater for Φ=0.5 than for Φ=0. This is in confirmation to the result mentioned earlier that an increase in the ambient humidity ratio will increase the value of M'_{excess}. As can be seen from Figure 4-9, the quantity of excess water decreases with the increase in excess air up to a pressure ratio of 2. Beyond a pressure ratio of 2, the pattern changes and the quantity of excess water decreases with excess air. This phenomenon becomes clearer when we examine Equation 3-9. Differentiating M'_{excess} with respect to y, assuming constant $M'_{liquid-out}$, we obtain the following:

$$dM'_{excess}/dy = \chi_{H_2O\text{-in}}/[2\chi o_2(1-\chi_{H_2O\text{-in}})] - \chi_{H_2O\text{-out}}/[2\chi o_2(1-\chi_{H_2O\text{-out}})] \quad 4\text{-}1$$

When the mole fraction of water in the depleted air is greater than that in the ambient air, the derivative of M'_{excess} with respective to y is negative and an increase in excess air decreases the quantity of excess water. The opposite effect is seen when $\chi_{H_2O\text{-out}}$ is less than $\chi_{H_2O\text{-in}}$. Physically, when $\chi_{H_2O\text{-out}}$ is greater than $\chi_{H_2O\text{-in}}$, some portion of the water generated inside the fuel cell is required to saturate a unit mass of depleted air. An increase in y increases the mass flow rate of excess air. Hence additional water

would be required to saturate the flow of depleted air. Consequently the amount of excess water generated decreases.

When $\chi_{H_2O\text{-out}}$ is less than $\chi_{H_2O\text{-in}}$, the amount of vapor present per unit mass of ambient air is more than what is required to saturate a unit mass of depleted air. Hence, upon pressurization, water is condensed from the air. An increase in *y* and hence an increase in the mass flow rate of air results in more water being removed from the depleted air. Hence the quantity of excess water increases. It should be noted that this trend is valid for all values of $M'_{liquid-out}$, provided its value is independent of *y*.

In order to determine the set of values of design parameters for which water balance is not achieved for all values of $M'_{liquid-out}$ under the worst case of dry ambient conditions. Equation 3-9 (Section 3.1) was used. At $M'_{liquid-out}$=0, when Φ=0, $\chi_{H_2O\text{-in}} = 0$, thus $M'_{excess} = 1 - \chi_{H_2O\text{-out}}(1+y-\chi o_2)/2\chi o_2$. Water balance is not achieved at steady state when M'_{excess}<0, that is when

$$1 - \{\chi_{H_2O\text{-out}}(1+y-\chi o_2)/2\chi o_2(1-\chi_{H_2O\text{-out}})\} < 0 \qquad 4\text{-}2$$

For $\chi_{O_2} = 0.21$, the above inequality becomes

$$\chi_{H_2O\text{-out}} > 0.42/(1.21+y) \qquad 4\text{-}3$$

The above inequality indicates a relation between $\chi_{H_2O\text{-out}}$ (which depends on the depleted air temperature and pressure) and excess air *y*. Figure 4-10 gives a plot of $\chi_{H_2O\text{-out}}$ versus *y* in which the region above the curve represents the operating conditions under which excess water is not produced. Approximating depleted air to be an ideal gas

$\chi_{H_2O\text{-out}}$ is the ratio of the partial pressure of vapor to the total pressure of depleted air ($\chi_{H_2O\text{-out}}$ =p_2/p_t). Hence water balance is not achieved for all values of $M'_{liquid-out}$ when

$$p_2 / p_t > 0.42/(1.21+y) \qquad 4\text{-}4$$

For a non-pressurized system operating at sea level (p_t=1 atmosphere), when y=0, p_2<0.347 atm which corresponds to a saturation temperature of 346 K. When y increases, the maximum limit of p_2 decreases and the corresponding saturation temperature decreases. Hence for a non-pressurized system operating at sea level, the maximum limit of depleted air temperature is approximately 346 K (73 °C). Similarly, for an altitude of 12000 feet, p_t= 0.6368 atm and the maximum limit of depleted air temperature is approximately 336 K.

Using Equation 4-4 one can thus determine the approximate maximum limit of depleted air temperature for different operating and ambient pressure conditions.

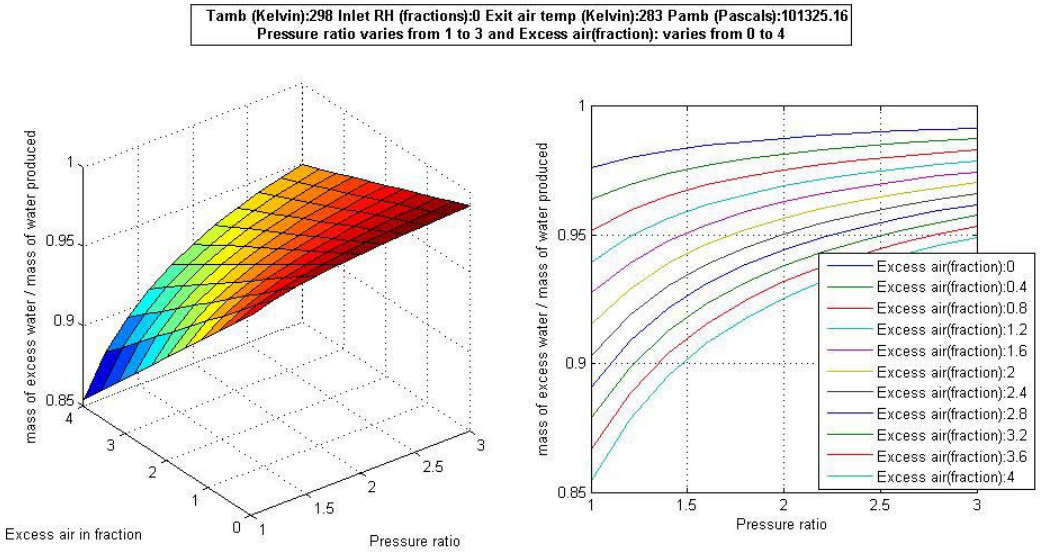

Figure 4-1. Excess water versus pressure ratio and fraction of excess air: sea level, very low depleted air temperature case

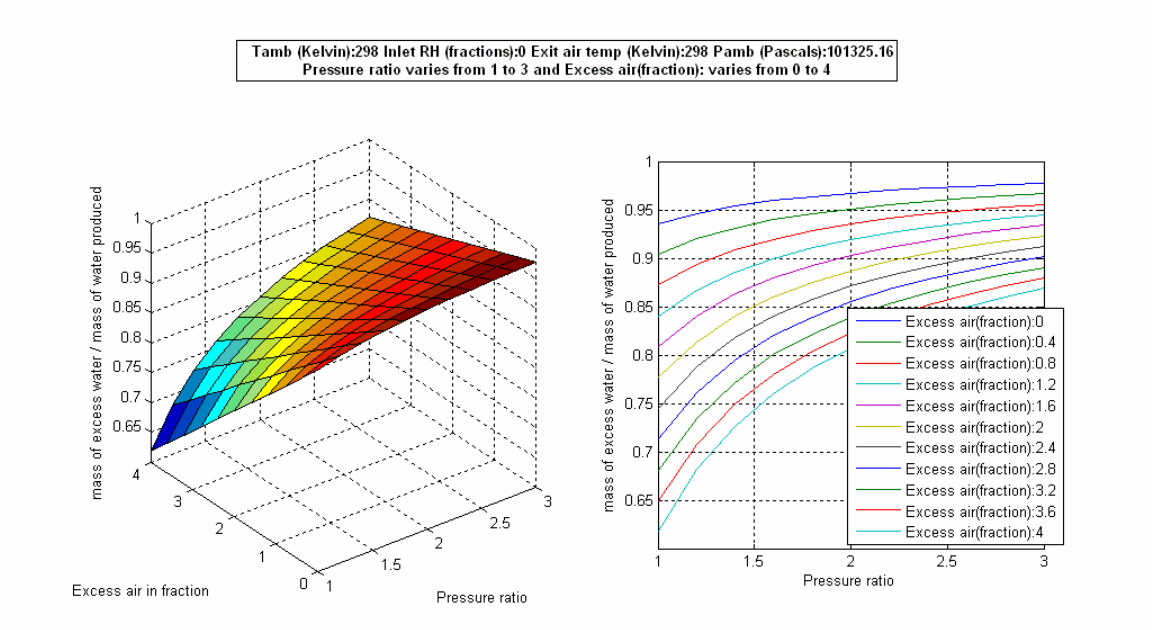

Figure 4-2. Excess water versus pressure ratio and fraction of excess air: sea level, low depleted air temperature case

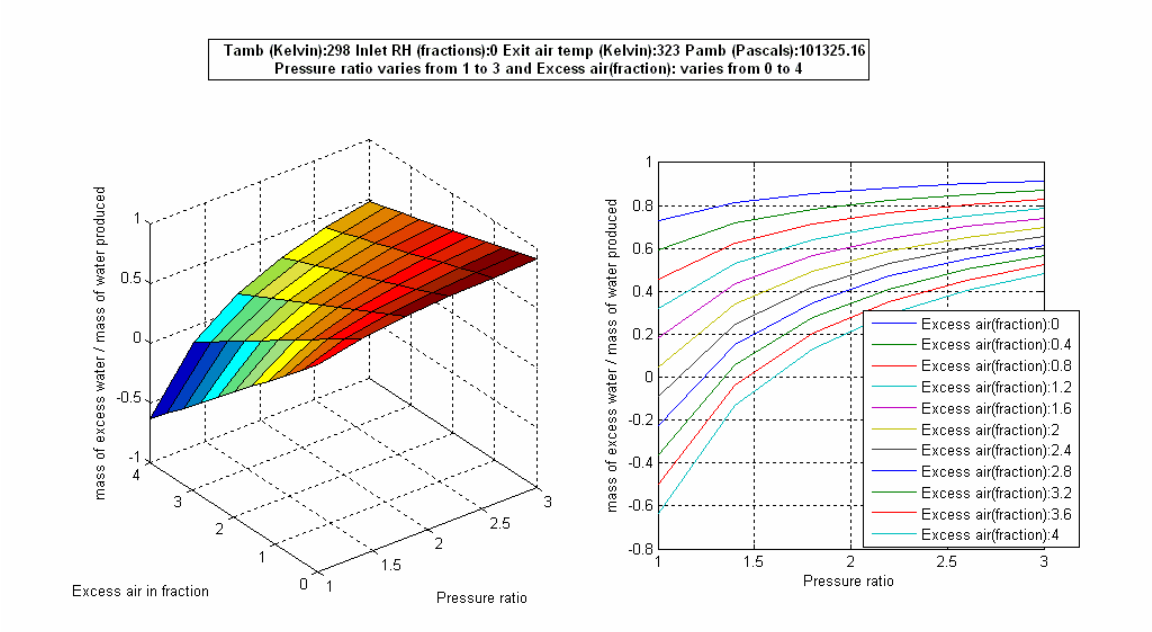

Figure 4-3. Excess water versus pressure ratio and fraction of excess air: sea level, intermediate depleted air temperature case

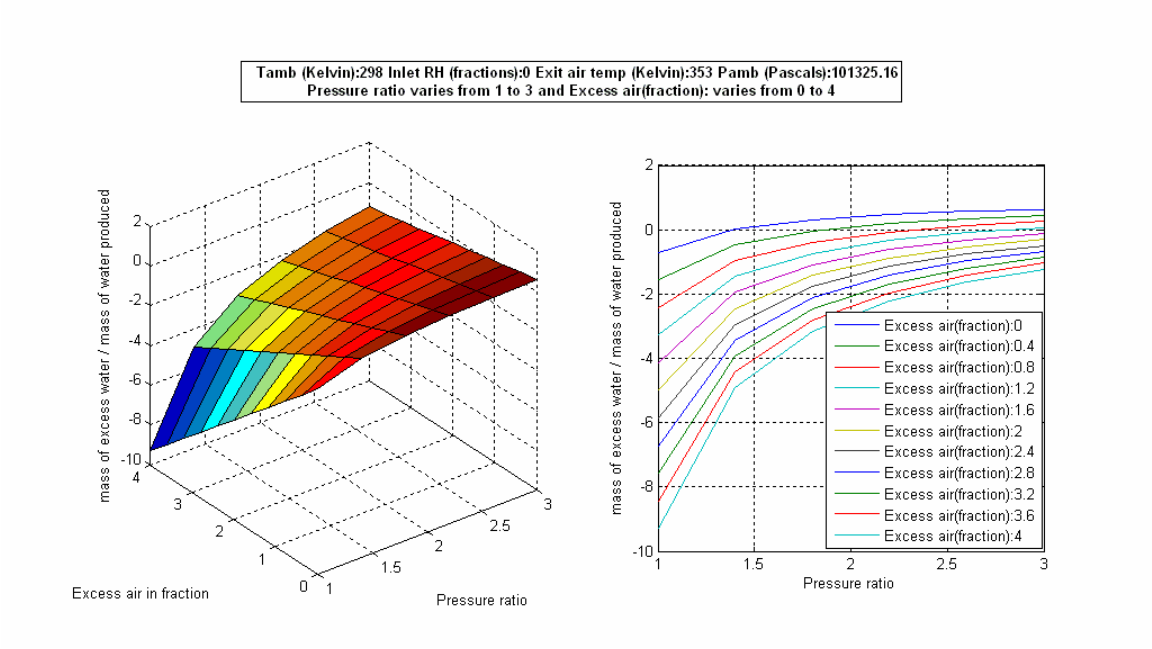

Figure 4-4. Excess water versus pressure ratio and fraction of excess air: sea level, high depleted air temperature case

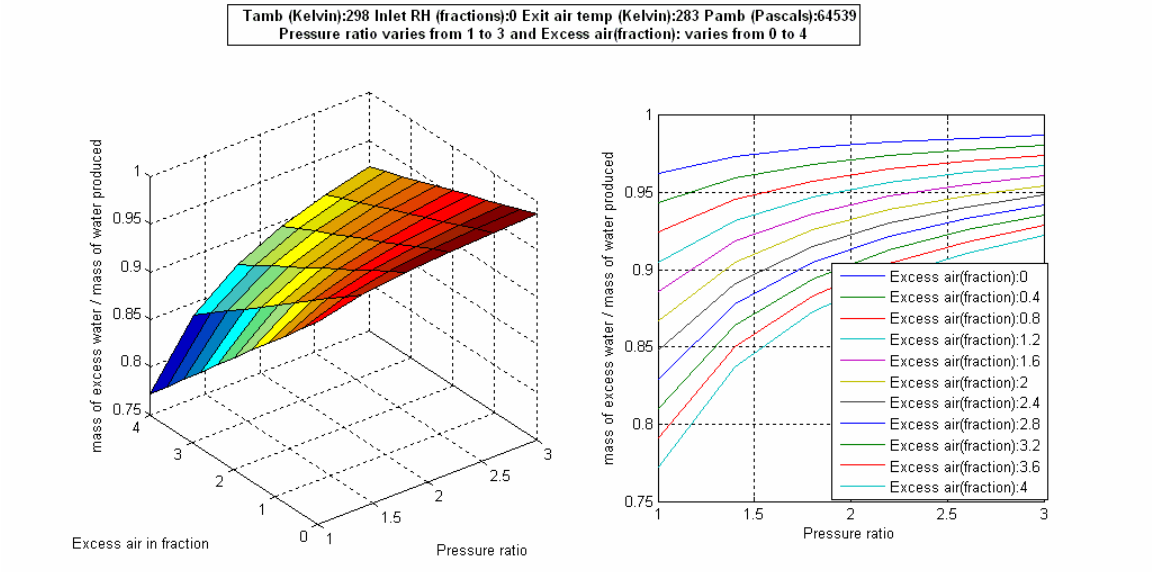

Figure 4-5. Excess water versus pressure ratio and fraction of excess air: high altitude, very low depleted air temperature case

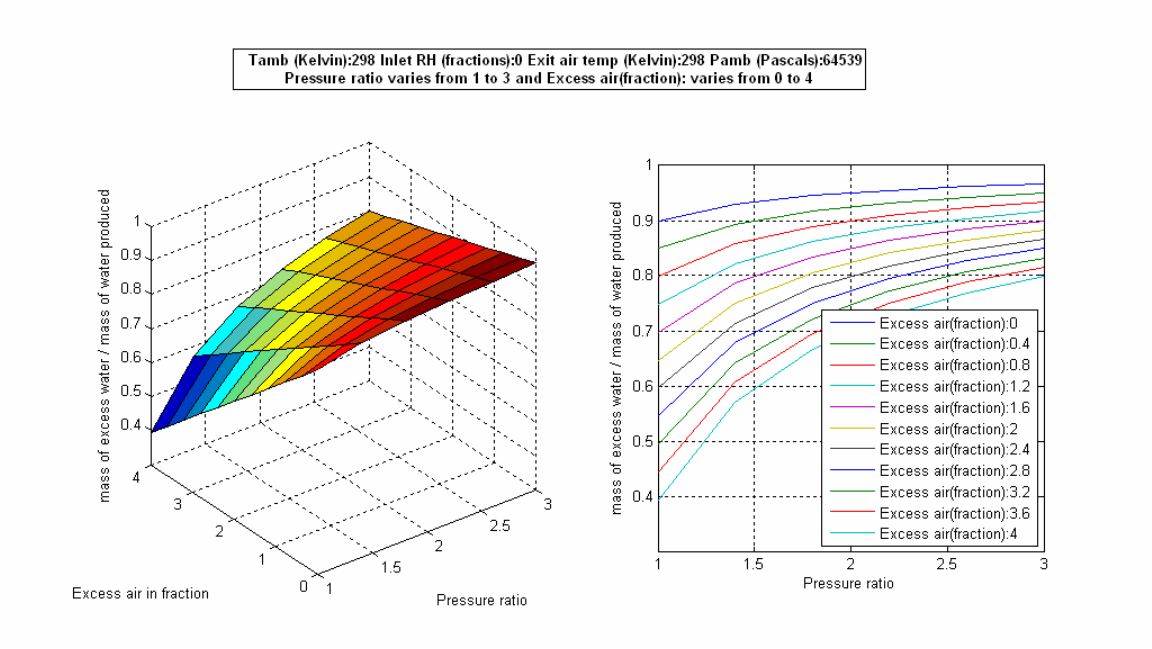

Figure 4-6. Excess water versus pressure ratio and fraction of excess air: high altitude, low depleted air temperature case

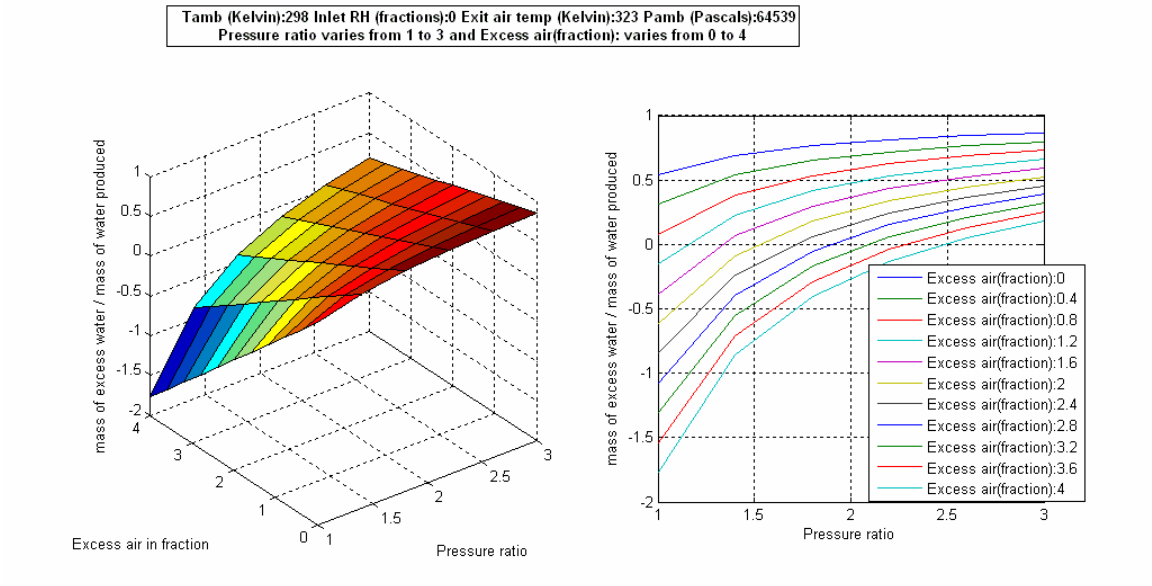

Figure 4-7. Excess water versus pressure ratio and fraction of excess air: high altitude, intermediate depleted air temperature case

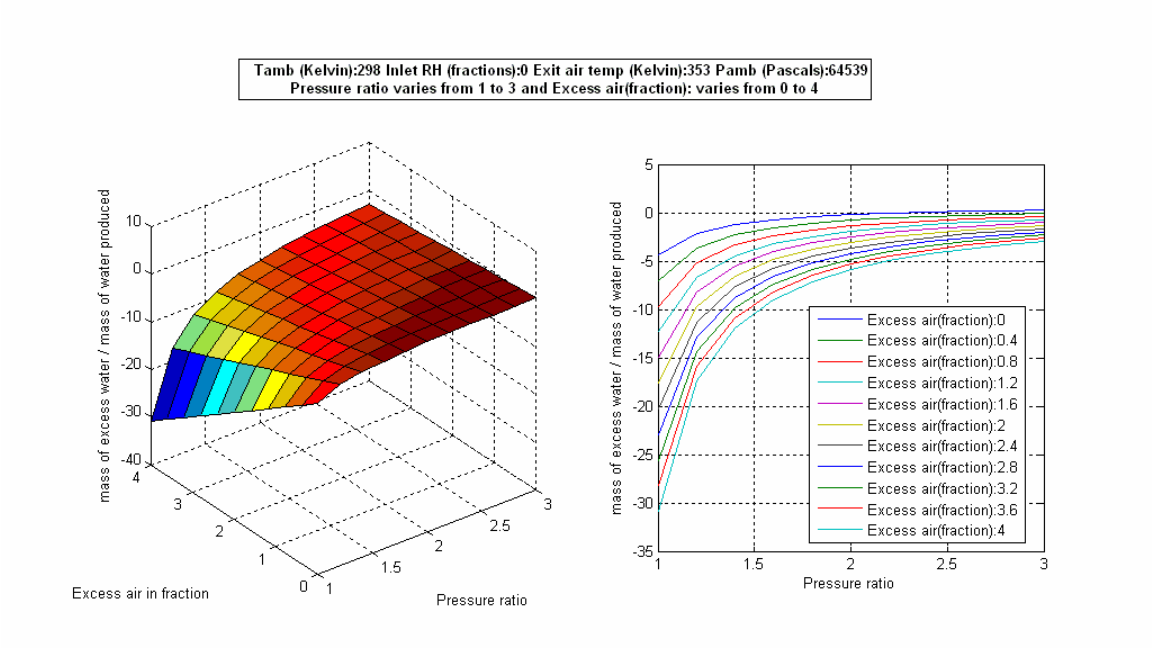

Figure 4-8. Excess water versus pressure ratio and fraction of excess air: high altitude, high depleted air temperature case

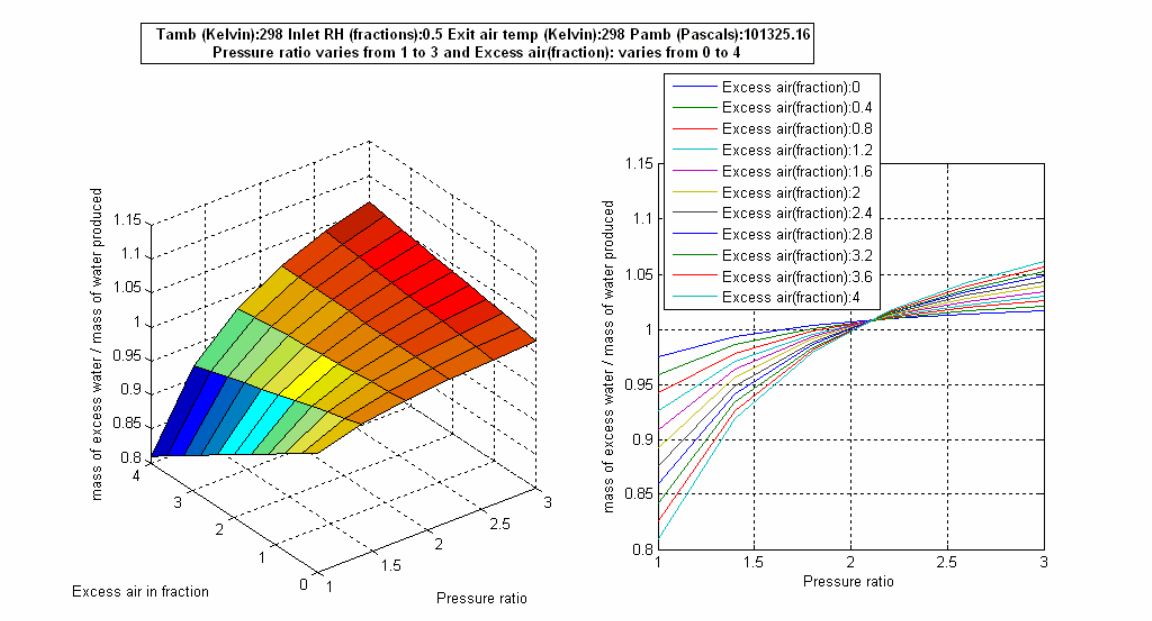

Figure 4-9. Excess water versus pressure ratio and fraction of excess air: sea level, low depleted air temperature, humid ambient air case

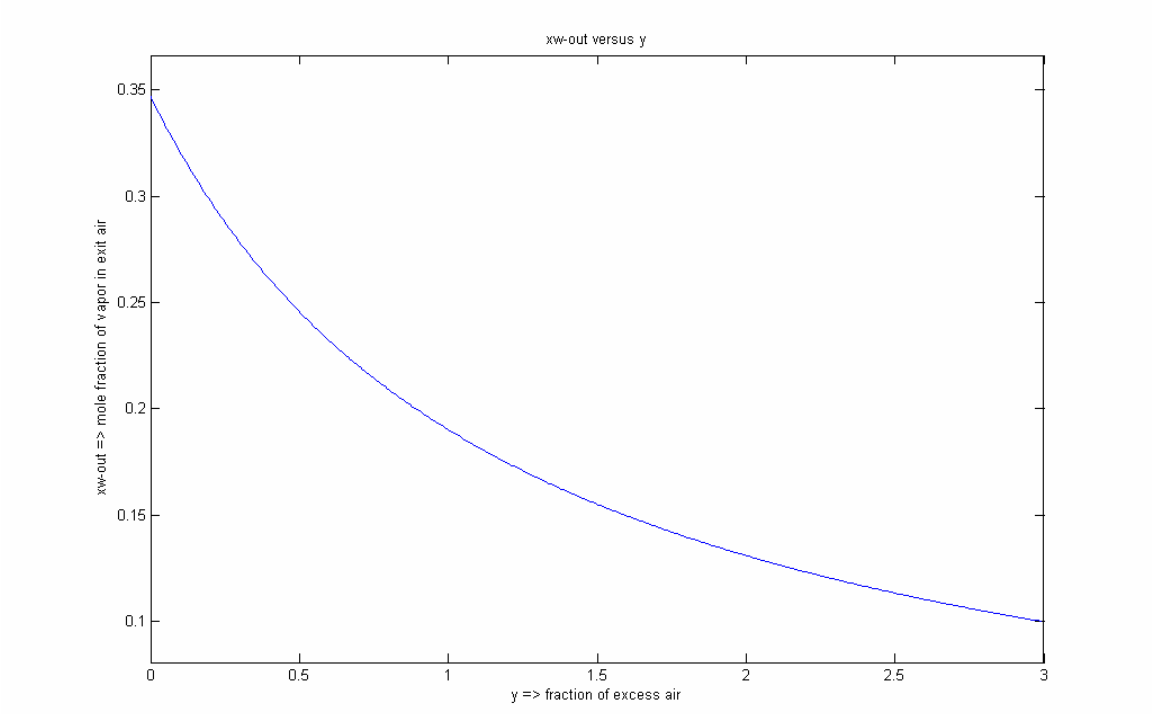

Figure 4-10. Excess water versus pressure ratio and fraction of excess air: sea level, low depleted air temperature, humid ambient air case

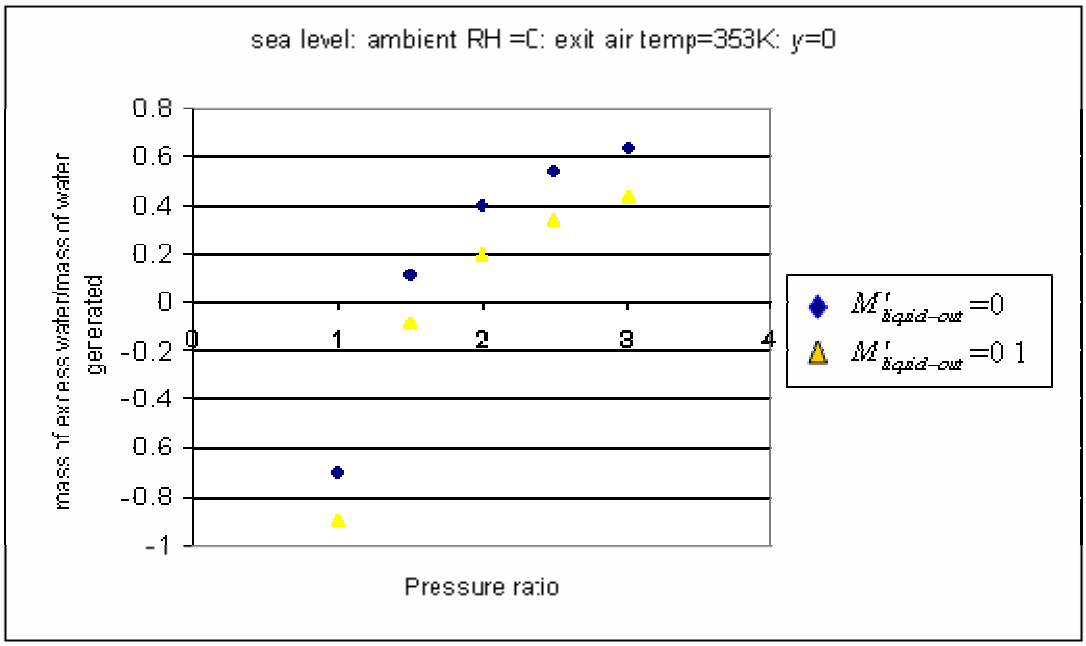

Figure 4-11. Excess water versus pressure ratio for $M'_{liquid-out}$ =0 and $M'_{liquid-out}$ =0.1: sea level, high depleted air temperature.

CHAPTER 5
EFFECT OF CERTAIN NON-IDEAL COMPONENTS ON WATER BALANCE MODEL INPUTS

As mentioned previously in chapter 3, M'_{excess} can be calculated from the water balance model when ambient conditions and design parameters are provided as inputs. The water balance model is independent of the choice of equipment. Any combination of equipment that leads to a same set of values of the design parameters yields the same result of M'_{excess} from the water balance model, for constant ambient conditions. Thus the choice of equipment affects the inputs to the water balance model and not the model itself.

The non-ideal nature of various components and sub-systems affects the design parameters of the fuel cell system, and hence the inputs to the water balance model. The effects on model inputs under varying operating conditions, when non-ideal air delivery sub-system and water recovery components are a part of the PEM fuel cell system, have been studied in this chapter.

5.1 Effect of a Non-Ideal Air Handling System on Model Inputs

The air handling system uses equipment like a blower or compressor to supply air for the electrochemical reaction and if required pressurize the stack. The non-ideal nature of the system varies certain operating parameters and hence affects the inputs to the water balance model. The changes in the model inputs due to the non-ideal behavior of the air-handling are as follows:

- Change in the depleted air pressure due to change in pressure ratio developed by a compression device under varying operating conditions.
- Change in the fraction of excess air at part load conditions due to the in-ability of the air supply device to reduce the mass flow rate of air below a certain limit.
- In ability of the air supply equipment to supply sufficient air quantity to all parts of the stack for lower mass flow rates of air. This forces the air handling system to maintain a minimum rate of air supply which results in an increase in the fraction of excess air at part load conditions.

Each of the above-mentioned changes in the model inputs and the resulting impact on water balance has been discussed in the subsequent sections of this chapter.

5.1.1 Change in Pressure Ratio Developed by a Non-ideal Air Compressor and Its Effect on Water Balance

For a pressurized stack, the depleted air pressure depends on the pressure ratio developed by the compression device. An ideal compressor would maintain a constant pressure ratio at all operating conditions. However for a non-ideal compressor, the pressure ratio and hence the depleted air pressure generally varies with the change in the mass flow rate of air through the compressor. Changing depleted air pressure, p_t, an input to the model, changes the value $\chi_{H_2O\text{-}out}$ and hence the amount of excess water generated by the system. Thus the extent to which pressurization affects water balance depends on the pressure ratio achieved by the equipment at a particular rotational speed and air mass flow rate. These performance characteristics vary with the type of equipment used and its geometry. For the current analysis a centrifugal compressor developed by Allied Signal Aerospace[17] was considered. The change in pressure ratio and hence water balance of a PEM based fuel cell stack was analyzed, when this device used for pressurization operated at part load conditions. It was assumed that the pressure at a location just downstream of the compressor was equal to the pressure of the depleted air.

5.1.1.1 Performance characteristics of an Allied Signal compressor at part load conditions

The performance characteristics of a centrifugal compressor are generally represented in terms of a compressor map which is a plot of pressure ratio versus corrected mass flow rate at various corrected rotational speeds. Corrected mass flow rate, $m^{\bullet}_{correct}$ is $m^{\bullet}_{a}\sqrt{\Theta}/(\delta\gamma_1^2)$ and corrected rotational speed, $N_{correct}$ is $N/\sqrt{\Theta}$, where $m^{\bullet}_{a}$ and N are the actual mass flow rate of air and actual rotational speed of the compressor respectively. The parameter Θ is the ratio of inlet air temperature to reference temperature. The variable δ is the ratio of inlet air pressure to reference pressure and γ_1 is the ratio of dimensional parameters. The value of γ_1 is useful for comparing two different dimensionally similar compressors. When the performance characteristic of a particular compressor is analyzed, the value of γ_1 is 1.

Figure 5-1 shows the compressor map of the centrifugal compressor used in the current analysis. The reference temperature and pressure for this Allied Signal compressor are 298K and 101.32 kPa. The red markings on the plot are the actual operating points at different rotational speeds and the blue lines are curefits to the data, generated by Jensen and Kristensen nonlinear curve fitting method.[24] These lines are constant corrected speed lines and represent the variation of pressure ratio with corrected mass flow rate for a particular rotational speed.

The green colored line on the left hand side of the map is the surge limit of the compressor and the one on the right hand side indicates the stall limit. It is generally recommended that centrifugal compressors should operate in the region between their surge limit and the stall limit on the compressor map, which, in case of the Allied Signal

compressor, is between the two green lines. Operating outside this region would lead to unsteady operation of the compressor.

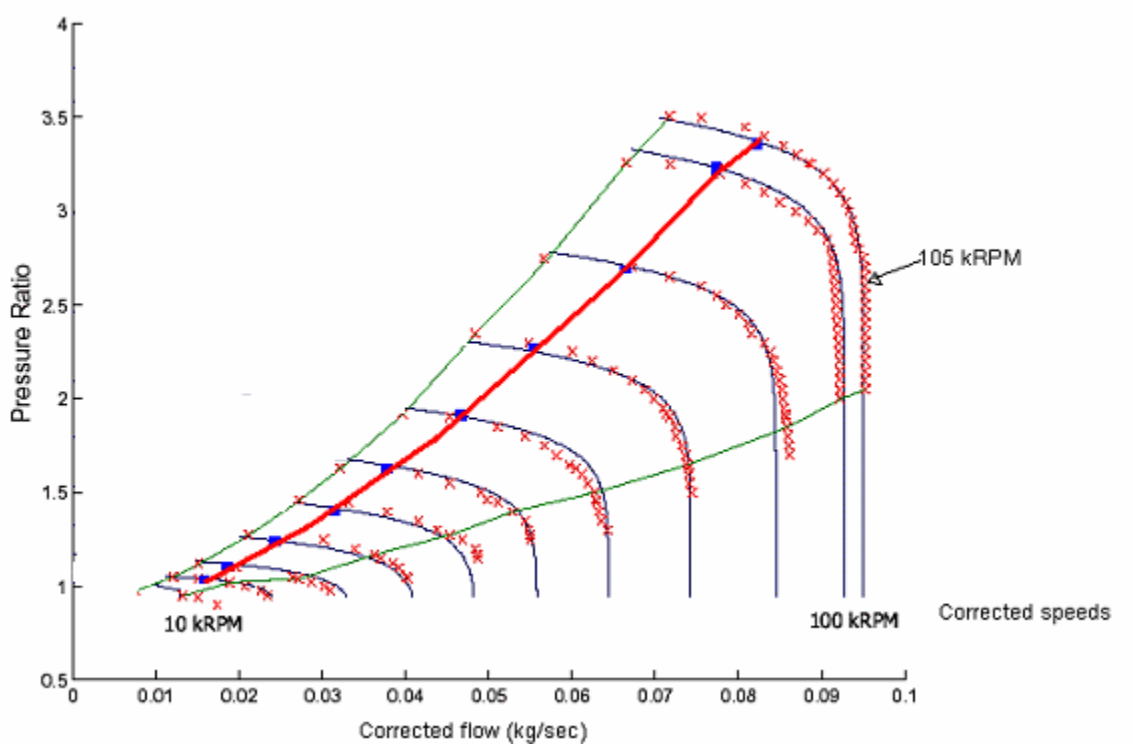

Figure 5-1. Compressor map of an Allied Signal compressor. (Source: Control-oriented modeling and analysis for automotive fuel cell systems, Pukrushpan J.T., Peng H., and Stefanopoulou A.G. Figure modified to represent the operating line on the compressor map)

The actual points on the map along which the compressor operates at various speeds depend on the resistance offered by the system, (which in our analysis is a fuel cell stack and its connecting piping) to which it is supplying compressed air. However, the system resistance offered by a stack and its connecting piping can be varied by adding one or more valves anywhere in the system and varying the closure of each valve or by varying the pipe size. Hence an operating line on a compressor map defines the system resistance offered at various operating conditions but does not limit it to a particular stack. In other words, the analysis is independent of the design of the fuel cell stack.

For the current analysis, the Allied Signal compressor is assumed to operate at a margin of 15% from the surge limit. This means that at a particular rotational speed, the mass flow rate of air through the compressor is 15% greater than the mass flow rate at the surge limit corresponding to that rotational speed. It can be seen from Figure 5-1 that when the operating point moves closer to the surge limit, higher pressure ratios can be achieved for the same rotational speed. However, operating close to the surge line involves the risk of the operating point crossing the surge limit, putting the compressor in the regime of unsteady operation. It is due to these factors that the compressor was assumed to operate at a 15% surge limit. The 15% surge limit line, which can also be referred to as the operating line of the compressor, has been indicated by a solid red line in Figure 5-1.

As shown in Figure 5-1, the constant speed lines for the compressor are plotted at different corrected rotational speeds starting from 10 kRPM reaching up to 105 kRPM. The design point of operation of the compressor in the current analysis is the one that lies at the intersection of the operating line (15% surge limit line) and the 105 kRPM constant corrected speed line. The fuel cell was assumed to produce maximum/design current when the compressor operates at this point. For analyzing the effect of water balance when the Allied Signal compressor is used as a compression device, 10 different points along the operating line of the compressor were selected. These points also include the design point of the compressor. They are indicated in Figure 5-1 as blue squares. The first three columns in Table 5-1 indicate the values of various parameters like normalized air flow rate, pressure ratio and corrected speeds at each of these points.

As mentioned earlier, the fuel cell is assumed to produce maximum current when the compressor operates at its design point. A drop in the speed of the compressor along the assumed operating line would reduce the mass flow rate and pressure of the air at the inlet of the fuel cell. This can be observed from parameters at various operating points depicted in Table 5-1. The current generated by the stack is directly proportional to the mass flow rate of air entering the stack. As the normalized mass flow rate of air at the 10 operating points are known, these points can be represented in terms of fraction of the design/ maximum stack current. The relation between stack current and normalized mass flow rate of air is explained below.

Table 5-1. Values of different parameters at the 10 selected operating points of an Allied Signal compressor

Normalized flow (kg/s)	**Pressure ratio**	**Corrected speed (kRPM)**	**Normalized flow/ Design normalized flow**
0.014	1.033	20	0.1759
0.017	1.104	30	0.2132
0.025	1.237	40	0.3034
0.031	1.420	50	0.3782
0.038	1.641	60	0.4661
0.046	1.900	70	0.5629
0.055	2.248	80	0.6684
0.066	2.712	90	0.8135
0.078	3.195	100	0.9577
0.082	3.374	105 (Design point)	1

5.1.1.2 Relation for fraction of design current

The current generated in a PEM based fuel cell is given by the equation[11]

$$I = 4F N_{O_2} / ń \qquad 5\text{-}1$$

where F is the faraday constant, n is the number of fuel cells in the stack and N_{O_2} is molar flow rate of oxygen in moles/sec that is effectively used by the fuel cell to produce water. It can be seen from Equation 3-4 that the number of moles of hydrogen required to

produce water is twice the number of moles of oxygen. In other words $N_{H_2}=2\,N_{O_2}$. Hence Equation 5-1 can be written as

$$I= 2F\,N_{H_2} / ń \qquad 5\text{-}2$$

Based on Equation 3-5, the molar flow rate of air entering the control volume and eventually the fuel cell is equal to $(1+y)N_{H_2}/2\chi o_2$. The molecular weight of ambient air for a standard composition of 21% mole fraction of oxygen and 78% mole fraction of nitrogen is 28.97. Hence the mass flow rate of air entering the compressor and eventually the fuel cell stack can be represented by the equation.

$$\dot{m}_a = 28.97\frac{(1+y)N_{H_2}}{2\chi_{O_2}} \qquad 5\text{-}3$$

Comparing Equations 5-2 and 5-3 we can represent $m_a^{\bullet}$ in terms of I as follows.

$$\dot{m}_a = 28.97\frac{(1+y).I.n}{4.F.\chi_{O_2}} \qquad 5\text{-}4$$

The value of n_{cell} remains constant for a particular fuel cell stack and, F and χ_{O_2} are constants. Thus the ratio stack current to the design stack current can be represented by

$$I / I_{design} = \frac{\dot{m}_a(1+y_{design})}{(1+y)\dot{m}_{a-design}} \qquad 5\text{-}5$$

Here, $\dot{m}_a$, I and y are mass flow rate of air, stack current and fraction of excess air respectively at any operating point of the compressor. Variables $\dot{m}_{a-design}$, I_{design} and y_{design} are the mass flow rate, stack current and fraction of excess air corresponding to the design point of the compressor.

The corrected mass flow rate $\dot{m}_{correct}$ is given by $\dot{m}_a \sqrt{\Theta}/(\delta\gamma_1^2)$. For constant ambient conditions, the values of Θ, δ and γ_1 remain constant for the Allied Signal compressor. Thus Equation 5-5 can be written as

$$I / I_{design} = \frac{\dot{m}_{correct}(1 + y_{design})}{(1 + y)\dot{m}_{correct-design}} \qquad 5\text{-}6$$

$\dot{m}_{correct-design}$ is the corrected mass flow rate at the design point.

Here y and y_{design} are inputs to the water balance model. The values of the ratio $\dot{m}_{correct}/\dot{m}_{correct-design}$ at all the 10 operating points have been indicated in the fourth column of Table 5-1. Each of the 10 operating points can thus be indicated in terms of fraction of design current provided, the value of y at each of these points is known. The values of the pressure ratios at these operating points can be used to provide input to the model and the value of M'_{excess} can be calculated for a given set ambient conditions and depleted temperatures (T_1). Thus the variation of M'_{excess}, when an Allied Signal compressor is used and the stack current and fraction of excess air (y) change from their design values, can be observed.

As explained in section 3.2 for the case when an Allied Signal compressor is used as a compression device, M'_{excess} can be plotted as a function of fraction of design stack current when y is known at all operating points and ambient conditions and depleted air temperature is provided as input.

5.1.1.3 Variation of M'_{excess} with fraction of design current for part load operation of an Allied Signal compressor

As explained earlier, the performance characteristics of an Allied Signal compressor decide the values of depleted air pressure (an input to the model) when the compressor operates at part load conditions. When the value of *y* (another input to the model) is known at all operating points of the compressor, M'_{excess} can be plotted as a function of fraction of design current. For the current analysis, it was assumed that the value of *y* does not change from its design value at all operating points of the compressor.

Figure 5-2 compares the plot of M'_{excess} versus fraction of design current for an Allied Signal compressor with that of an ideal compressor. The graphs are plotted for different values of design excess air fraction (y_{design}). The depleted air temperature (T_1) was assumed to be equal to 323K and the ambient conditions were assumed as follows: T_a = 298K, Φ=0, p_{amb}=101325.16 Pa (sea level). The value of $M'_{liquid-out}$ was assumed to be zero. Figure 5-3 is similar to Figure 5-2 except that plots correspond to a higher value of T_1 which is equal to 353K. Figures 5-4 and 5-5 are similar to Figures 5-2 and 5-3 respectively, except that the values of M'_{excess} were calculated assuming that the fuel cell operates at 12000 feet instead of sea level (i.e. p_{amb}=64539 Pa).

A few trends are common amongst all four figures. First one is that for an Allied Signal compressor, M'_{excess} decreases along the constant excess air lines with the decrease in fraction of design current. From Equation 5-5, when the value of *y* remains constant at its design value, the stack current is directly proportional to the mass flow rate of air. A decrease in the fraction of design stack current decreases the mass flow rate of air through the stack. A drop in the value of mass flow rate of air through the compressor

along its operating line decreases the pressure ratio across the stack. This in turn drops the depleted air pressure. As explained in section 4.1, a drop in the depleted air pressure decreases the value of M'_{excess} at all times. Thus M'_{excess} decreases with the decrease in stack current. In comparison, the value of M'_{excess} for an ideal compressor stays constant, along the constant *y* lines, with the change in fraction of design current. This is because the pressure ratio developed by an ideal compressor stays constant at all mass flow rates.

Another trend that is observed in Figures 5-2 through 5-5 is that an increase in the value of y_{design} decreases the value of M'_{excess}, both for an ideal and a non-ideal compressor. The variation of M'_{excess} with excess air fraction is governed by Equation 4-1. For the case where Φ=0, the value of M'_{excess} always decreases with the increase in the fraction of excess air.

A third trend common to all four figures is that the value of M'_{excess} for the non-ideal compressor, drops more rapidly, with the decrease in the fraction of design current, for higher fractions of excess air than for lower ones. Moreover the difference between the constant 'fractions of excess air' lines increases. A drop in the stack current results in a lower depleted air pressure and hence a drop in the rate at which excess water is produced for a unit mass of ambient air supplied. An increase in the value of *y* increases the mass flow rate of ambient air. As a result the drop in the rate of excess water production is magnified and the constant fraction of excess air lines tend to move farther away from each other. This can also be seen from Equation 3-9; a drop in the pressure ratio drops the value of $\chi_{H_2O\text{-out}}$ and hence M'_{excess}. Now an increase in value *y* further magnifies this effect resulting in steeper lines of constant *y*. It should be noted that the trends described above

do not change for all values of $M'_{liquid-out}$, provided $M'_{liquid-out}$ stays constant all operating points of the compressor.

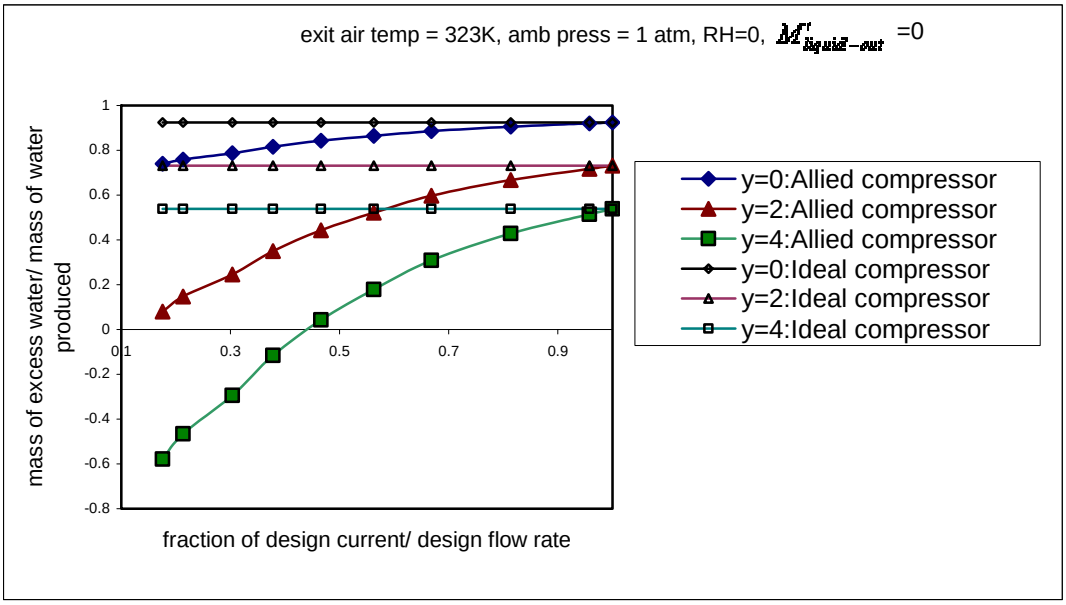

Figure 5-2. Excess water versus fraction of design current and fraction of excess air: sea level, intermediate depleted air temperature, $M'_{liquid-out}$=0

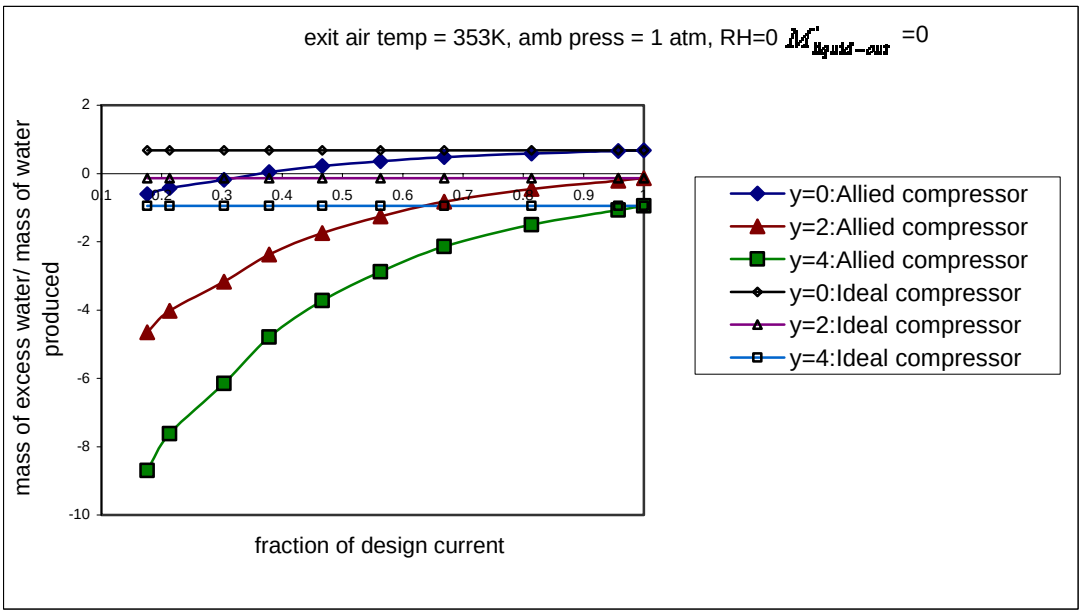

Figure 5-3. Excess water versus fraction of design current and fraction of excess air: sea level, high depleted air temperature, $M'_{liquid-out}$=0

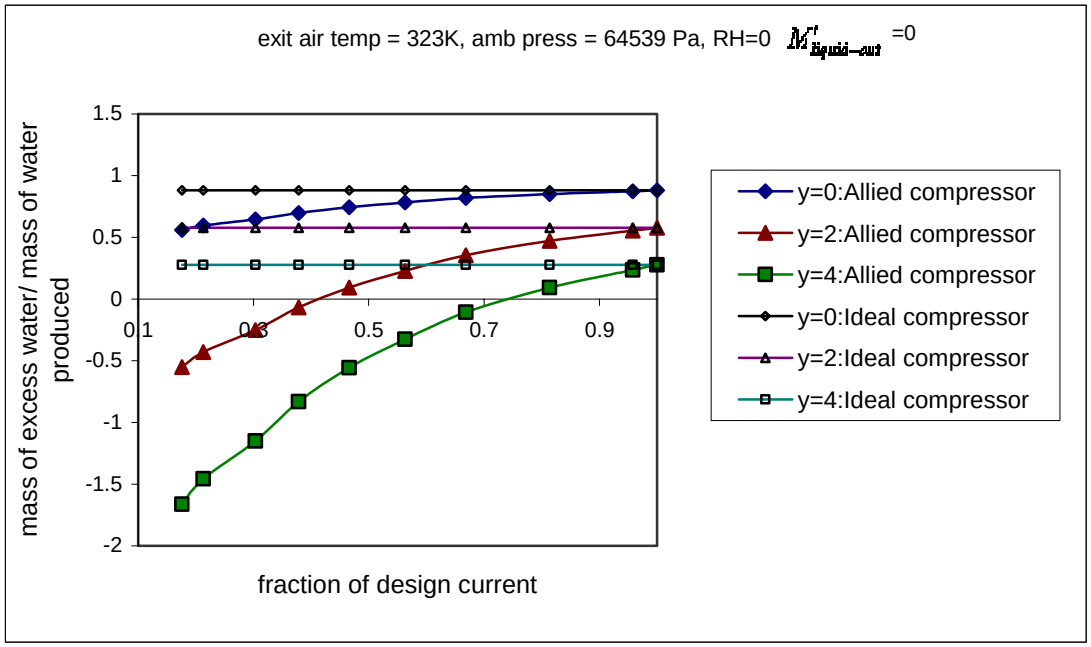

Figure 5-4. Excess water versus fraction of design current and fraction of excess air: high elevation, intermediate depleted air temperature, $M'_{liquid-out}$ =0

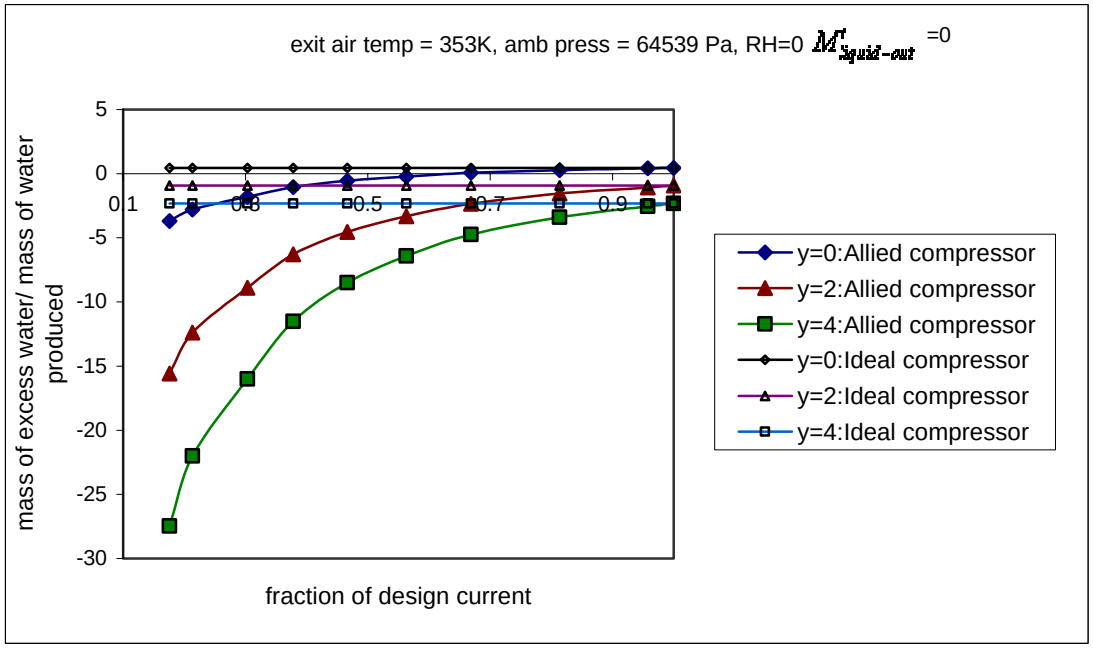

Figure 5-5. Excess water versus fraction of design current and fraction of excess air: high elevation, high depleted air temperature, $M'_{liquid-out}$ =0

5.1.2 Change in Fraction of Excess Air due to Compressor Limitations

A drop in the mass flow rate of air through a non-ideal compressor decreases the pressure ratio developed by it. Thus one of the inputs to the model, the depleted air pressure, is governed by the characteristics of a compressor. This has also been seen in section 5.1.1 for the case of an Allied Signal compressor. Most compression devices are unable to maintain stable operation when the mass flow rate of air drops below a certain limit. Hence it is recommended that the mass flow rate of air through a compressor should not drop below a certain minimum value. This limits the ratio $\dot{m}_{correct}/\dot{m}_{correct-design}$ to a minimum value. If the fraction of excess air is maintained at its design value at all operating points of the compressor, the minimum mass flow rate of air through a compressor corresponds to a minimum value of fraction of design current. Based on Equation 5-6, if current must be dropped below this minimum value, y must be increased above its design value. As the fraction of design current decreases the value of y increases. Thus the value of y (another input to the model) under the condition of low current is governed by the minimum mass flow rate of air that a compressor can supply under stable operation. To summarize, the values of two of the inputs of the model namely depleted air pressure and fraction of excess air are dependent on the performance of the compressor.

Figure 5-6 shows the variation of y with respect to the fraction of design current when an Allied Signal compressor is used to pressurize a stack. The minimum ratio of $\dot{m}_{correct}/\dot{m}_{correct-design}$ for stable operation of the Allied Signal compressor is 0.176 which corresponds to a pressure ratio of about 1. The value of y is assumed to stay constant at its design value of 0.8 until the ratio of $\dot{m}_{correct}/\dot{m}_{correct-design}$ drops to the minimum value of

0.176. A constant value of *y* implies that the fraction of design current is equal to the ratio $\dot{m}_{correct}/\dot{m}_{correct-design}$ based on equation 5-6. For fractions of design current lower than this point, the mass flow rate of air stays constant and the value of *y* increases from its design value. Figure 5-6 shows that a drop in the fraction of design current below 0.176 results from an increase in the value of *y*. A zero current is never achieved in this case as it would correspond to a value of *y* reaching infinity.

Figure 5-7 shows the variation of M'_{excess} versus fraction of design current. The ambient temperature, pressure and relative humidity were assumed to be 298 K, 1 atmosphere and 0% and the depleted air temperature was assumed to be 323 K. The value of $M'_{liquid-out}$ was assumed to be zero in this case. It can be seen that for fractions of design current greater than 0.176, the value of M'_{excess} decreases due to a drop in pressure ratio. When the fraction of design current increases beyond 0.176, the pressure ratio stays constant at its minimum value of 1 and the value of *y* increases (as shown in Figure 5-6) An increase in *y* when ambient air relative humidity is zero, decreases the value of M'_{excess} as seen in Figure 5-7.

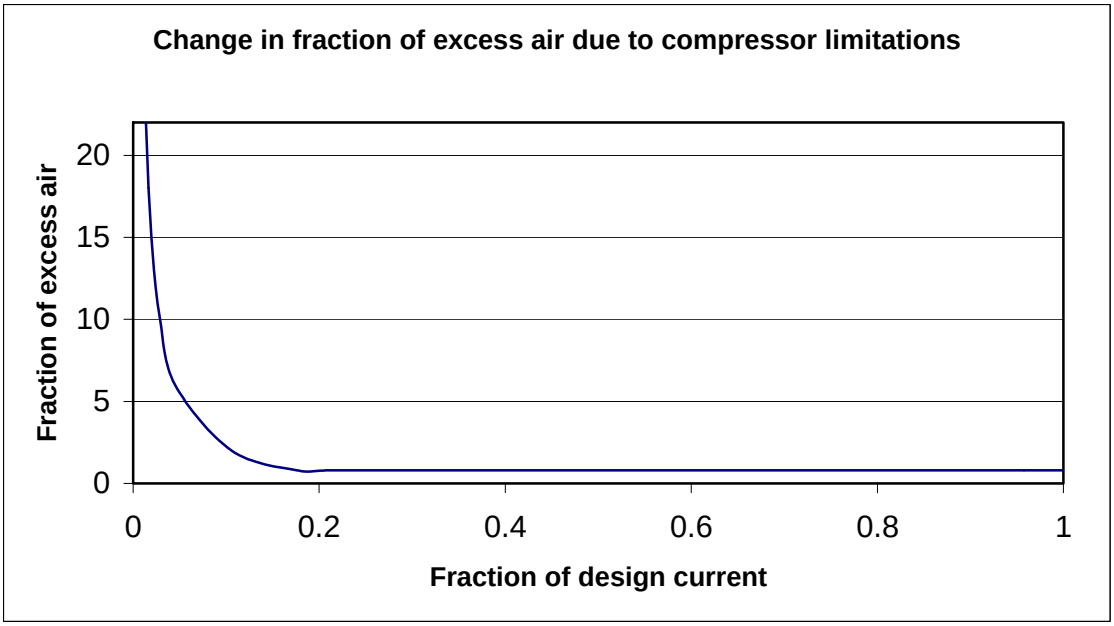

Figure 5-6. Change in fraction of excess air due to compressor limitations for lower fractions of design current.

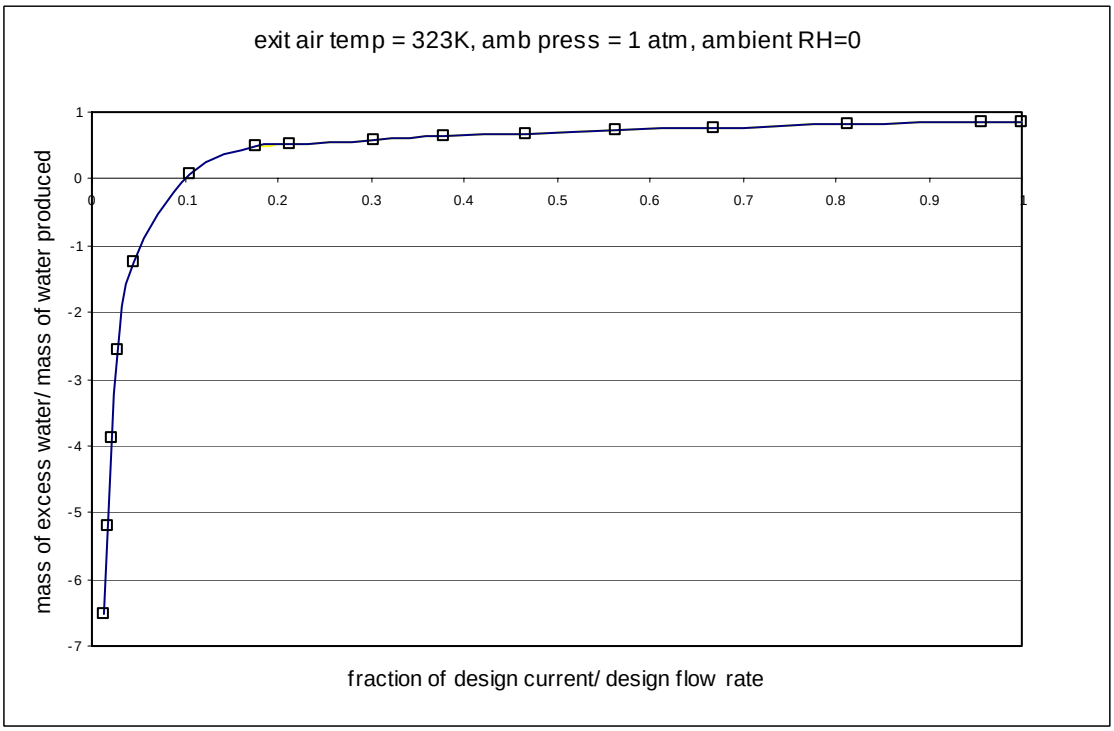

Figure 5-7. Excess water versus fraction of design current: compressor limitation: sea level, intermediate depleted air temperature, $M'_{liquid-out}$=0

5.1.3 Change in Fraction of Excess Air due to Air Distribution Limitations

A conventional PEM fuel cell stack consists of a number of cells that are electrically connected together. In order to ensure adequate supply of air to all cells in the stack, a certain minimum flow of air should be supplied to the stack. This limits the value of the ratio $\dot{m}_{correct}/\dot{m}_{correct-design}$ and fraction of design current for constant value of *y*. The minimum flow of air supply required by the stack is generally higher than the minimum possible air that the compressor can supply. The effect of limiting the air supply to a minimum value, as discussed in section 5-1-2, is that the value of *y* must be increased beyond its design value to achieve lower fractions of current. Thus the value of one of the model inputs *y* is also governed by the air distribution limitations in the stack.

Figure 5-8 shows the variation of *y* with the change in fraction of design current when an Allied Signal compressor is used to pressurize the stack. It was assumed that the minimum value of the ratio of corrected mass flow rate of air, $\dot{m}_{correct}/\dot{m}_{correct-design}$ required by the stack was 0.3. Here again, the value of *y* stayed constant for fractions of design current greater than 0.3. When, the value of the fraction of design current decreases below 0.3, the value of *y* increases. Figure 5-9 shows the variation of M'_{excess} with fraction of stack current. The ambient conditions and design parameters like depleted air temperature, $M'_{liquid-out}$ and y_{design} and were assumed to be same as in case of Figure 5-7. It can be seen from Figure 5-9 that M'_{excess} decreases with the decrease in fraction of design current due to the change in pressure ratio for $\dot{m}_{correct}/\dot{m}_{correct-design}$ greater than 0.3. Until this point, the fraction of design current is equal to $\dot{m}_{correct}/\dot{m}_{correct-design}$. The value of *y* must be increased beyond its design value for fractions of design current lower than 0.3. The

result as shown in Figure 5-9 is that M'_{excess} progressively decreases with the increase in y. Figure 5-10 shows the plots in Figures 5-7 and 5-9 super-imposed on each other. It can be seen that the value of M'_{excess} starts decreasing earlier due to stack limitations. This is because the minimum mass flow rate of air required by the stack is higher than the minimum mass flow rate of stable operation of the compressor in this case. Thus the value y starts decreasing earlier due to stack limitations, resulting in an earlier drop of M'_{excess}.

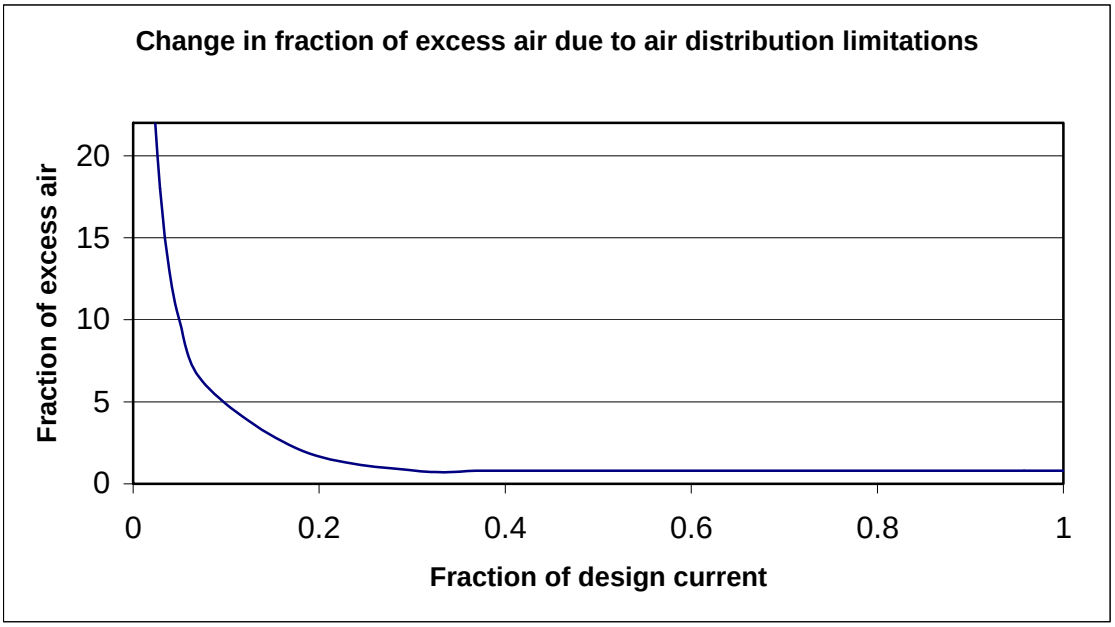

Figure 5-8. Change in fraction of excess air due to air distribution limitations for lower fractions of design current.

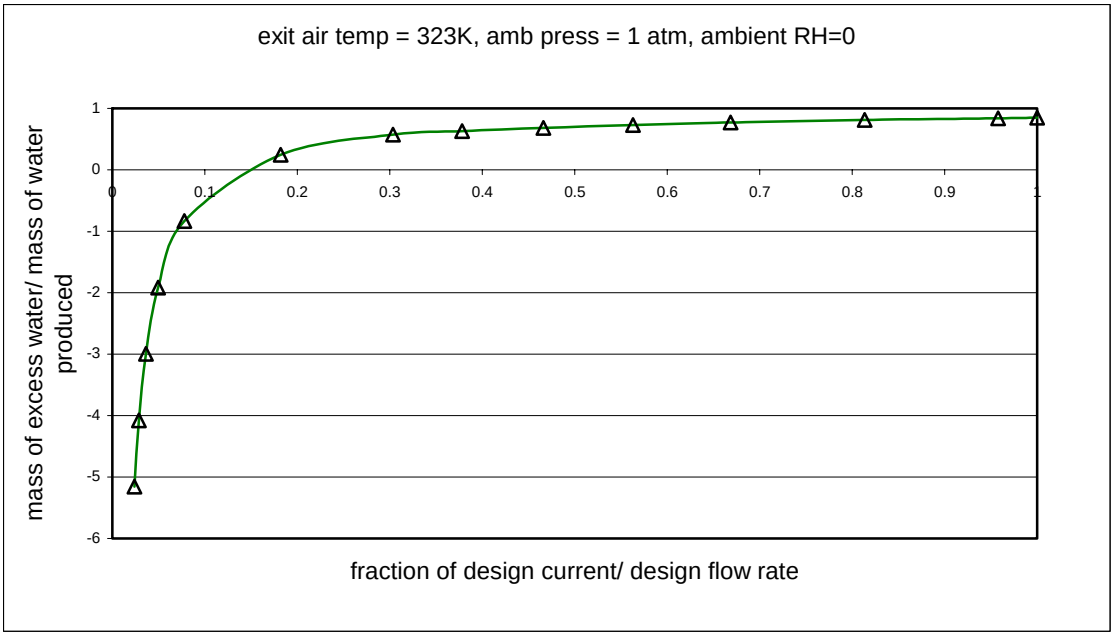

Figure 5-9. Excess water versus fraction of design current: air distribution limitation: sea level, intermediate depleted air temperature, $M'_{liquid-out}$=0

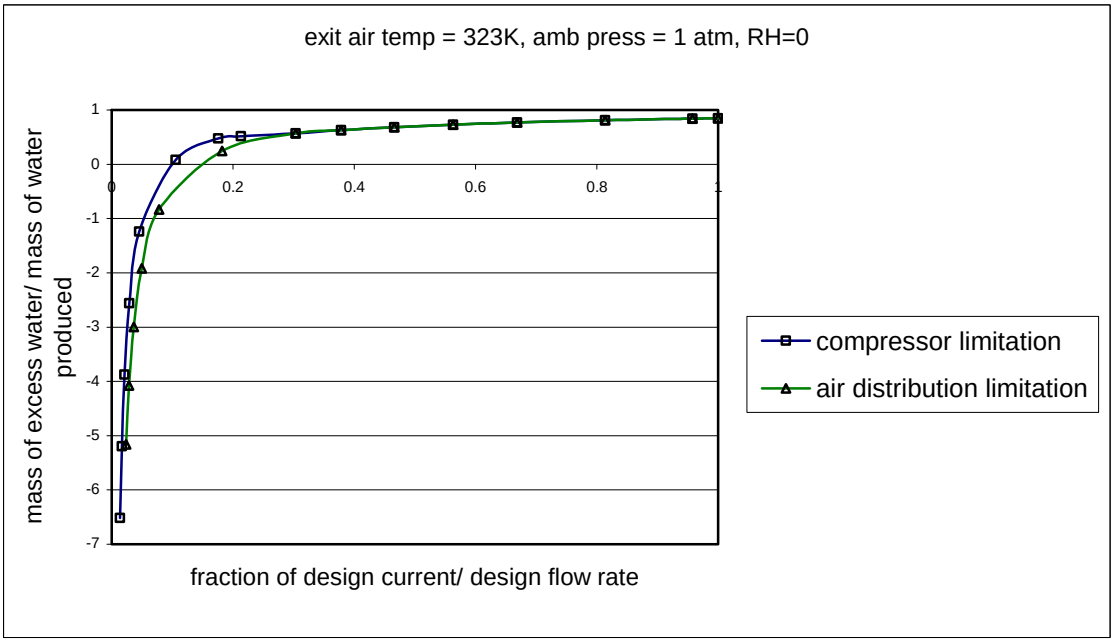

Figure 5-10. Excess water versus fraction of design current: comparison of air distribution limitation versus compressor limitation: sea level, intermediate depleted air temperature, $M'_{liquid-out}$=0

5.2 Effect of Non-Ideal Water Separator on Water-Balance Model Inputs

An ideal water separator, having an efficiency of 100%, would separate all the liquid water from the depleted air. Hence the mass flow rate of un-recovered liquid in this case would be zero. In other words, the value of $M'_{liquid-out}$ for an ideal water separator would be zero for all operating and ambient conditions. However, the efficiency of a realistic water separator is less than 100% as some liquid water cannot be recovered from the depleted air. The value of $M'_{liquid-out}$ in this case would be greater than zero. Thus the value of $M'_{liquid-out}$, an input to the water balance model, depends on the efficiency of the water separator device.

5.2.1 Relation between $M'_{liquid-out}$ and η

In order to find a relation between $M'_{liquid-out}$ and η, a separate control volume was drawn just around the water separator device. As explained in chapter 3, part of the liquid water separated from the depleted air is supplied back to the stack to maintain the humidity of the membranes. Let $\dot{m}_{mem}$ represent the mass flow rate at which liquid water is supplied back to the stack. The remaining portion is either discharged to the ambient or stored in a storage device at a mass flow rate of $\dot{m}_{H_2O-excess}$. The mass flow rate of liquid water that could not be separated in the water separator is represented by $\dot{m}_{liquid-out}$. Figure 5-11 shows the control volume drawn around the water separator and also indicates the various flow streams of water entering and leaving the control volume. The mass flow rate of water leaving the water separator and also the control volume is

$\dot{m}_{H_2O-excess} + \dot{m}_{mem} + \dot{m}_{liquid-out}$. The control volume around the water separator is assumed to be at steady state for the current analysis. Consequently, the mass flow rate at which liquid water enters the control volume equals the mass flow rate at which it leaves. The mass flow rate at which liquid water enters the water separator and hence the control volume is thus equal to $\dot{m}_{H_2O-excess} + \dot{m}_{mem} + \dot{m}_{liquid-out}$. This can also be seen from Figure 5-11.

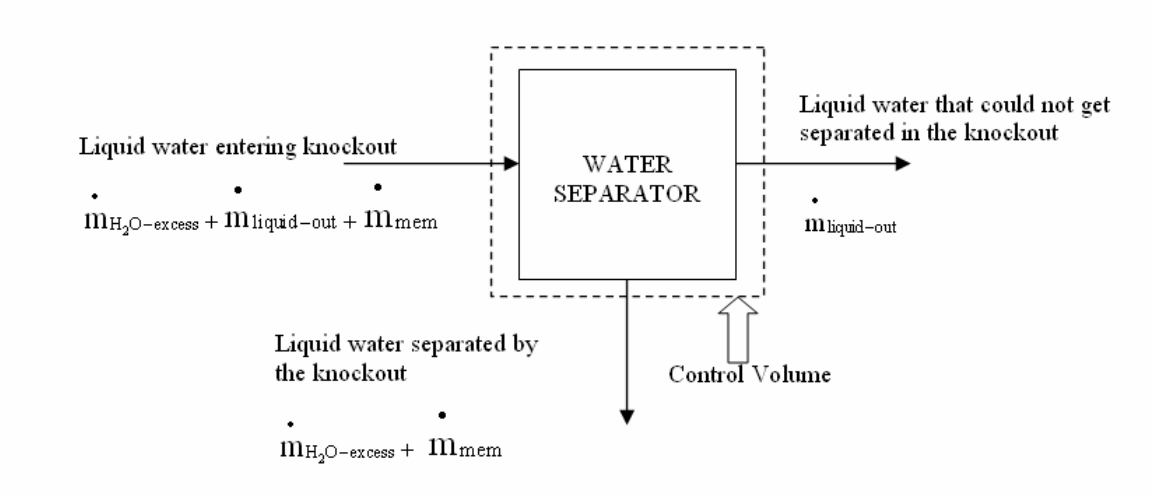

Figure 5-11. Mass flow rate of water entering and leaving the water separator and the control volume

The efficiency of the water separator device η may be defined as

$$\eta = \frac{\text{liquid water separated by the water separator}}{\text{liquid water entering the water separator}} \qquad 5\text{-}8$$

Based on Figure 5-11, η can be written as

$$\eta = \frac{\dot{m}_{mem} + \dot{m}_{H_2O-excess}}{\dot{m}_{mem} + \dot{m}_{H_2O-excess} + \dot{m}_{liquid-out}} \qquad 5\text{-}9$$

Dividing the numerator and denominator with $\dot{m}_{H_2O\text{-}gen}$ we obtain the following:

$$\eta = \frac{(\dot{m}_{mem} / \dot{m}_{H_2O\text{-}gen}) + M'_{excess}}{(\dot{m}_{mem} / \dot{m}_{H_2O\text{-}gen}) + M'_{excess} + M'_{liquid-out}} \quad 5\text{-}10$$

Let $(\dot{m}_{mem} / \dot{m}_{H_2O\text{-}gen})$ be defined as the non-dimensional membrane flow term, represented by the variable M'_{mem}. Rearranging Equation 5-10 we obtain the following:

$$M'_{liquid-out} = \frac{(M'_{mem} + M'_{excess})(1\text{-}\eta)}{\eta} \quad 5\text{-}11$$

Equation 5-11 relates the non-dimensional un-separated liquid water term to the water separator efficiency in terms of the non-dimensional membrane flow and excess flow terms.

In order to show the effect of using a non-ideal water separator on water balance, specific design of the fuel cell system was considered and the value of $M'_{liquid-out}$ and M'_{excess} calculated for a certain set of operating and ambient conditions.

5.2.2 Design Case

The value of $M'_{liquid-out}$ is related to the water separator efficiency by Equation 5-11. The value of M'_{excess} is given by Equation 3-9 and its value can be calculated from the model for known values of $M'_{liquid-out}$. Substituting Equation 3-9 in Equation 5-11 we obtain the following:

$$M'_{liquid-out} = (1\text{-}\eta)\left\{M'_{mem} + 1 + \left[\frac{\chi_{H_2O\text{-}in}(1+y)}{2\chi_{O_2}(1\text{-}\chi_{H_2O\text{-}in})}\right] - \left[\frac{\chi_{H_2O\text{-}out}(1+y-\chi_{O_2})}{2\chi_{O_2}(1\text{-}\chi_{H_2O\text{-}out})}\right]\right\} \quad 5\text{-}12$$

Here, the values of $\chi_{H_2O\text{-}in}$ and $\chi_{H_2O\text{-}out}$ can be calculated using a procedure similar to the one described in chapter 3 when ambient conditions and depleted air temperature and pressure are provided as input. The values of y and χ_{O_2} are inputs as in case of the model

developed to calculate M'_{excess} . The value of M'_{mem} varies with the operating conditions and the design of the fuel cell stack and its auxiliaries.

The current analysis assumes that the overall system was designed such that the ambient air entering the stack first is pressurized and heated up to depleted air pressure and temperature respectively. The air then is humidified to 90% relative humidity after which it contacts the electrodes and participates in the electrochemical reaction. It was also assumed that humidifying the ambient air to 90% relative humidity at depleted air temperature and pressure ensures that the membranes reach a steady state and don't lose or gain any water. The mass flow rate at which water is supplied back to the stack ($\dot{m}_{\text{mem}}$) is equal to the mass flow rate of water required to humidify the ambient air to 90% relative humidity at depleted air temperature and pressure. The value of M'_{mem} can be determined for a given set of ambient and operating conditions and $M'_{liquid-out}$ can also be calculated.

As can be seen from Equation 3-5, the mass flow rate of water entering the control volume in the form of vapor, as a part of the ambient air is

$$\dot{m}_{H_2O\text{-in}} = M_w \chi_{H_2O\text{-in}} (1+y) N_{H_2} / [2\chi_{O_2} (1 - \chi_{H_2O\text{-in}})]$$

where $\chi_{H_2O\text{-in}}$ is the mole fraction of vapor present in the ambient air. Ambient air that is pressurized and heated to depleted air conditions and humidified up to 90% relative humidity shall be referred to as humidified air in the rest of the analysis. Let $\chi_{H_2O\text{-}90\%}$ represent the mole fraction of vapor present in the humidified air. As this process of humidification takes place before the electrochemical reaction, the mass flow rate of dry

air remains the same before and after humidification. Based on Equation 3-5 the mass flow rate of water flowing through the stack as a part of the humidified air is

$$\dot{m}_{humid} = \frac{M_w \chi_{H_2O\text{-}90\%} (1+y) N_H}{2\chi o_2 (1 - \chi_{H_2O\text{-}90\%})} \quad 5\text{-}13$$

The mass flow rate at which liquid water should be supplied to the stack, in order to humidify the ambient air ($\dot{m}_{mem}$), is the difference between $\dot{m}_{H_2O-in}$ and $\dot{m}_{humid}$, and is given by

$$\dot{m}_{mem} = \frac{M_w (1+y) N_H}{2\chi o_2} \left\{ \frac{\chi_{H_2O\text{-}90\%}}{(1 - \chi_{H_2O\text{-}90\%})} - \frac{\chi_{H_2O\text{-in}}}{(1 - \chi_{H_2O\text{-in}})} \right\} \quad 5\text{-}14$$

From Equation 3-9 and 5-14

$$M'_{mem} = \frac{(1+y)}{2\chi o_2} \left\{ \frac{\chi_{H_2O\text{-}90\%}}{(1 - \chi_{H_2O\text{-}90\%})} - \frac{\chi_{H_2O\text{-in}}}{(1 - \chi_{H_2O\text{-in}})} \right\} \quad 5\text{-}15$$

The value of χo_2 for ambient air is usually 0.21 and *y* is one of the inputs. The mole fraction of vapor in ambient air, $\chi_{H_2O\text{-in}}$, as explained in section 3.1, is calculated from Equation 3-10.

In order to calculate the value of $\chi_{H_2O\text{-}90\%}$, the modified saturation pressure of vapor in the humidified air (p_2) corresponding to depleted air temperature was calculated using the Poynting effect. The procedure to calculate p_2 is the same as explained in section 3.1. As the relative humidity of humidified air is 90%, the partial pressure of vapor present in the humidified air (denoted as p_{humid}) is 0.9 times p_2.

$$p_{humid} = 0.9\ p_2 \quad 5\text{-}16$$

As mentioned earlier in section 3.1, the mole fraction of vapor present in moist air is the ratio of the fugacity of the vapor at its partial pressure to the fugacity of the vapor at the total pressure of the mixture. Thus

$\chi_{H_2O\text{-}90\%} = f(p_{humid}, T_1)/f(p_t, T_1)$

The value of $\chi_{H_2O\text{-}90\%}$ was input in Equation 5-15 to calculate M'_{mem}.

The value of M'_{mem} was input in Equation 5-12 to calculate the value of $M'_{liquid-out}$ for a given set of design and operating conditions.

The value of $M'_{liquid-out}$ calculated using the procedure described above indicates the drop in the non-dimensional excess water term from its ideal value for the current design case and can be used to calculate M'_{excess} using model developed earlier in chapter 3.

5.2.3 Variation of M'_{excess} for the Design Case

As explained earlier, the value of $M'_{liquid-out}$ can be calculated for a specific design case where the value of $\dot{m}_{mem}$ was assumed to be equal to the mass flow rate of water required to humidify the ambient air to 90% relative humidity at depleted air temperature and pressure. The value of $M'_{liquid-out}$ can be provided as an input to the model and the value of M'_{excess} can be calculated for different ambient and operating conditions.

Figure 5-12 shows the plot M'_{excess} versus pressure ratio for the design case and compares it with the plot of M'_{excess} versus pressure ratio for the case where $M'_{liquid-out}$ stays constant at 0. The efficiency of the water separator was assumed to be 90% (η=0.9) and the ambient temperature, pressure and relative humidity were assumed to be 298K, 64.539 kPa (0.637 atmosphere) and 0% RH respectively. The depleted air temperature

was assumed to have a value of 353K which corresponds to the case of an un-cooled stack and the value of *y* was assumed to be 0.

Figure 5-13 is similar to figure 5-12 except that the value of depleted air temperature was dropped to 298K from 353K.

A trend that is common to both the figures is that the difference between M'_{excess} for the design case and M'_{excess} for the case where $M'_{liquid-out}$=0 (difference is equal to the value of $M'_{liquid-out}$ for the design case) stays approximately constant with the increase in pressure ratio for a constant value of *y*, and pressure ratio varying from 1 to 3. This effect results from a combination of two different factors. As mentioned in section 4.1, an increase in the pressure ratio increases the value of M'_{excess} and also the fraction of excess water that was not separated in the water separator, $\dot{m}_{liquid-out}$. This effect tends to increase the value of $M'_{liquid-out}$ with the increase in pressure ratio. An increase in pressure ratio also reduces the mole fraction of water present in air at 90% relative humidity corresponding to depleted air temperature and pressure ($\chi_{H_2O\text{-}90\%}$). This reduces the amount of water required to be supplied back to the stack (M'_{mem}) and hence decreases $M'_{liquid-out}$ based on Equation 5-15. The net effect is that the value of $M'_{liquid-out}$ remains more or less constant with the increase in pressure for the design case. This effect however is specific to the design case considered in Section 3.3.

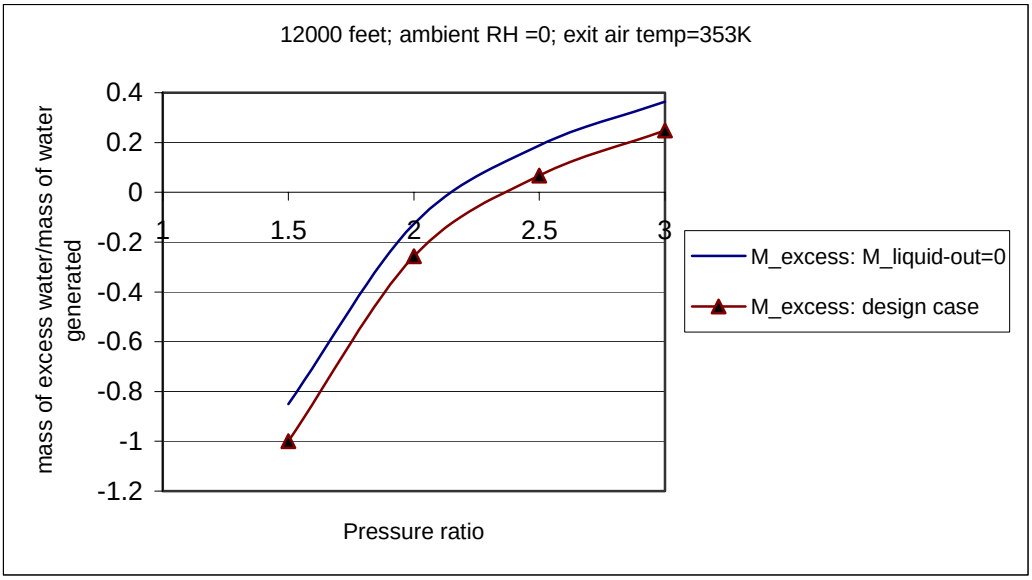

Figure 5-12. Variation of the excess water term with pressure ratio for $M'_{liquid-out}$=0 and the design case: high elevation, high depleted air temperature

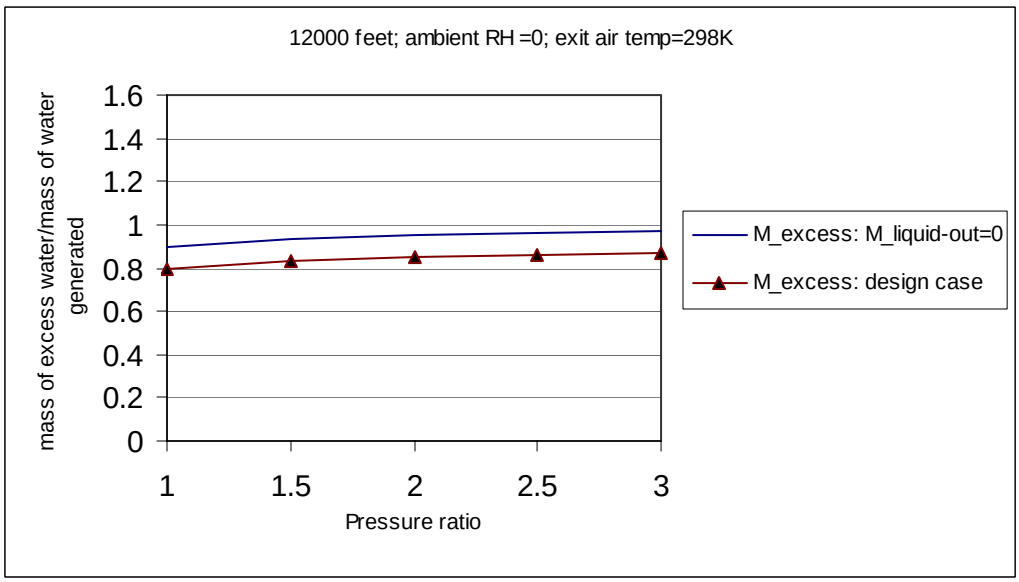

Figure 5-13. Variation of the excess water term with pressure ratio for $M'_{liquid-out}$=0 and the design case: high elevation, low depleted air temperature

CHAPTER 6
CONCLUSIONS

To ensure adequate humidification of the membranes, a steady state condition must be achieved in which excess water is always generated. To find the quantity of excess water, a water balance analysis was carried out for a control volume that circumscribed the fuel cell stack and most of its auxiliaries. The results of the analysis may be summarized as follows:

- A water balance model was developed that was able to calculate the excess water quantity when ambient conditions and design parameters – fraction of excess air, exhaust gas pressure and exhaust gas temperature – were provided as input.
- The sensitivity to each model input determined.
- The model developed was independent of the design of the fuel cell system in the sense that any combination of equipment or sub-system choices that lead to the same set of values of design parameters would yield the same result.

The model was used to calculate the values of excess water rate for different ambient and operating conditions. Based on the results of the model it can be concluded that

- Pressurizing the fuel cell stack or cooling the stack exhaust, or both, is recommended in order to achieve water balance in a PEM fuel cell operating at high altitudes when ambient air relative humidity is low.
- The rate at which excess water is produced increases with the increase in depleted air pressure for all ambient and design conditions.
- The rate of excess water increases with decreasing depleted air temperature for all ambient and design conditions
- An increase excess air decreases the rate of excess water production when ambient air relative humidity is zero. When the ambient relative humidity is greater than

zero, the trend of excess water rate versus excess air depends on the relative humidity of ambient air and depleted air pressure.

The non-ideal nature of various components and sub-systems affects the design parameters of the fuel cell system, and hence the inputs to the water balance model. To study the limitations imposed by a non-ideal air handling system on model inputs, the performance characteristics of an Allied Signal air compressor, typically chosen for fuel cell systems, were studied. Based on the study it was concluded that

- For a pressurized stack, the pressure ratio (and hence depleted air pressure) developed by a non-ideal compressor decreases with the decrease in the current generated by the stack. As a result, the rate at which excess water is produced decreases with the drop in stack current. Thus low-power and idle conditions represent the most difficult water balance challenge.

- Due to limitations imposed on the mass flow rate of air delivered by the compressor, the fraction of excess air must be increased in order to achieve a drop in stack current beyond a certain limit. The result is that the rate of excess water production decreases when the stack current falls beyond that limit, even though the depleted air pressure may remain the same. Therefore, low-power conditions would be even more challenging, using the design choice for stack pressurization.

To summarize, a fuel cell stack operating at low power conditions may encounter water balance problems at near-dry ambient conditions.

To study the effect of a non-ideal water separator on model inputs, a control volume analysis of the water separator was carried out. Based on the analysis it was determined that

- One of the inputs to the water balance model, the mass flow rate of liquid water that could not be recovered by the water separator, is directly proportional to the efficiency of the water separator.

- A decrease in the efficiency of the water separator decreases the rate at which excess water is produced, provided other operating parameters and design conditions are constant.

Hence, it can be concluded that the efficiency of the water separator affects the water balance in the fuel cell system.

CHAPTER 7
RECOMMENDATIONS

Based on the water balance analysis and its results, the following recommendations are being made for future work pertinent to the current area of study.

- - The water balance model discussed in this study was able to determine those operating conditions where water balance is not achieved. It is recommended that various options to improve water balance should be analyzed in order to determine the optimum choice for each set of operating conditions where water balance is not achieved. Here optimum choice refers to an option which results in maximum efficiency of the overall system.

  - Once the optimum choices for various operating conditions have been determined, different control schemes for various drive cycles should be formulated. These control schemes should be designed in a manner such that for a given set of ambient parameters and load conditions, the controller would vary the operating parameters of various equipments to achieve water balance in the most efficient manner.

- The current study does not take into account the effect of flooding. It is recommended that a parametric study be carried out on various fuel cells to determine the maximum value of the excess water rate beyond which flooding becomes more prominent in PEM fuel cells.

- The current water balance model is independent of the design of the system. It is only limited to the hydrogen oxidation reaction that take place inside the fuel cells. With minor modifications, the model can be applied to other energy conversion processes that involve oxidation of hydrocarbons to produce water. It is recommended that such an exercise be carried determine the potential of these energy conversion cycles to produce potable water along with electricity.

- The excess water generated by the fuel cell system can be used to cool the stack and the water separator. A thermodynamic analysis of such an arrangement can be carried out to provide inputs to the water balance model in order to determine the operating conditions under which water balance is achieved at steady state. The effect of non-ideal nature of heat exchanger can also be considered in this study.

LIST OF REFERENCES

1. Ebbing, D., General Chemistry, 3rd edition, Houghton Mifflin, Boston, 1990.

2. Atkins, P.W., Physical Chemistry, 3rd edition, W.H. Freeman and Company, New York, 1986.

3. EG & G Services Parson, Inc., Fuel Cell Handbook, 5th edition, U.S. Department of Energy, National Energy Technology Laboratory, Morgantown, 2000.

4. Kordesch, K.V., Survey of Carbon and Its Role in Phosphoric Acid Fuel Cells, Report Prepared for Brookhaven National Laboratory, 1979, BNL 51418.

5. Betts, D., Modeling and Analysis of Fuel Cell Engines for Transport Applications, Master's Thesis, University of Florida, Gainesville, 2000.

6. Yu, X., Zhou, B. and Sobiesiak, A., Water and thermal management for ballard PEM fuel cell stack, Journal of Power Sources, in press, 2005.

7. Haraldsson, K. and Alvfors, P., Effects of ambient conditions on fuel cell vehicle performance, Journal of Power Sources, in press, 2004.

8. Markel, T., Haraldsson, K. and Wipke, K., An analysis of water management for a PEM fuel cell system in automotive drive cycles, http://www.ctts.nrel.gov/analysis/pdfs/asme_rit_fc_conf_403_water_mgmt_paper.pdf, accessed Gainesville, July 2005.

9. Stumper, J., L¨ohr, M. and Hamada, S., Diagnostic tools for liquid water in PEM fuel cells, Journal of Power Sources, 143 (2005), 150–157.

10. Kreuer, K.D., Vielstich ,W., Lamm A. and Gasteiger, H., Handbook of Fuel Cells – Fundamentals, Technology Applications, Vol. 3, Part 3, John Wiley & Sons, Chichester, 2003.

11. Larmine, J. and Dicks A., Fuel Cell Systems Explained, 2nd edition, John Wiley & Sons, West Sussex, 2003.

12. Gelfi, S., Stefanopoulou, A.G., Pukrushpan, J. T. and Peng, H., Dynamics of low-pressure and high-pressure fuel cell air supply system, IEEE Proceedings of American Control Conference, Colorado, 2003, 2049-2054.

13. Cunningham, J. M., Air System Management for Fuel Cell Vehicle Applications, Master's Thesis, University of California, Davis, 2001.

14. Hussain, M. M., Baschuka, J. J., Li, X. and Dincer, I., Thermodynamic analysis of a PEM fuel cell power system, Journal of Power Sources, 44 (2005), 903–911.

15. Baschuk, J. J. and Li, X., Mathematical model of a PEM fuel cell incorporating CO poisoning and O_2 (air) bleeding, https://www.inderscience.com/browse/index.php?journalID=13, accessed Gainesville, May 2005.

16. Kulp, G. W., A Comparison of Two Air Compressors for PEM Fuel Cell Systems, Master's Thesis, Virginia Polytechnic Institute and State University, Blacksburg, 2001.

17. Stefanopoulou, A.G., Pukrushpan, J. T. and Peng, H., Control-oriented modeling and analysis for automotive fuel cell systems, Journal of Dynamic Systems, Measurement, and Control, 126 (2004), 14-25.

18. Ji, X., Lu, X. and Yan, J., Survey of experimental data and assessment of calculation methods of properties for the air–water mixture, Journal of Applied Thermal Engineering, 23 (2003), 2213–2228.

19. Xiaoyan Jia and Jinyue Yana, Saturated thermodynamic properties for the air–water system at elevated temperatures and pressures, Journal of Chemical Engineering Science, 58 (2003), 5069–5077.

20. Wark, K., and Richards, D.E., Advanced Thermodynamics for Engineers, 6th edition, McGraw-Hill, New York, 1999.

21. Reynolds, W.C., Physical Properties of 40 Substances in SI, Stanford University Press, Stanford, 1979.

BIOGRAPHICAL SKETCH

Rohit Sharma was born in Ahmedabad, India, on the 30th of April, 1980. Rohit completed his bachelor's degree from Sardar Patel University, Gujarat, India, on July 2001 after which he joined Alstom Projects India Ltd. as a systems design engineer. Rohit worked with the organization for duration of two years after which he decided to pursue his master's degree in mechanical engineering.

Rohit started working towards his master's at the University of Florida from the Fall of 2003. Later, he got the opportunity to be a part of the fuel cell lab under the guidance of Dr. W. E. Lear and Dr. James Fletcher. Upon completion of his master's in August 2003, Rohit plans to continue contributing to the energy industry and build on his knowledge and experience.